AD-A228 969

REPORT DOCUMENTATION PAGE

DTIC FILE COPY

Form Approved
OMB No. 0704-0188

1. AGENCY USE ONLY (Leave blank)	2. REPORT DATE	3. REPORT TYPE AND DATES COVERED
		Final Report/1 Oct 87-30 Sep 90

. TITLE AND SUBTITLE

Computer Simulations of Radiation Generation From Relativistic Electron Beams

5. FUNDING NUMBERS

61102F/2301/A8

. AUTHOR(S)

Anthony T. Lin

. PERFORMING ORGANIZATION NAME(S) AND ADDRESS(ES)

University of California
Department of Physics
Los Angeles, CA 90024-1547

8. PERFORMING ORGANIZATION REPORT NUMBER

AFOSR-TR- 90 1102

. SPONSORING/MONITORING AGENCY NAME(S) AND ADDRESS(ES)

AFOSR/NP
Bolling AFB DC 20332-6448

10. SPONSORING/MONITORING AGENCY REPORT NUMBER

AFOSR-88-0027

11. SUPPLEMENTARY NOTES

12a. DISTRIBUTION/AVAILABILITY STATEMENT

Approved for public release; distribution is unlimited.

12b. DISTRIBUTION CODE

13. ABSTRACT *(Maximum 200 words)*

In investigating the effects of magnetic field on the output power of a plasma-filled Backward Wave Oscillator, it was found that within a certain range of magnetic field the growth rate of beam-plasma cyclotron interaction is significantly larger than the conventional backward wave oscillation. Computer simulations of a 100 GHz electron cyclotron autoresonance master oscillator have been carried out that was designed for an experiment at the Naval Research Laboratory.

14. SUBJECT TERMS

Backward Wave Oscillator, Cyclotron Autoresonance Maser, Magnicon

15. NUMBER OF PAGES

21

16. PRICE CODE

UL

17. SECURITY CLASSIFICATION OF REPORT	18. SECURITY CLASSIFICATION OF THIS PAGE	19. SECURITY CLASSIFICATION OF ABSTRACT	20. LIMITATION OF ABSTRACT
UNCLASSIFIED	UNCLASSIFIED	UNCLASSIFIED	SAR

Computer Simulations of Radiation Generation From Relativistic Electron Beams

AFOSR 88-0027 Final Technical Report

Anthony T. Lin
UCLA Physics Department

University of California at Los Angeles
Department of Physics
Los Angeles, CA 90024-1547

COMPUTER SIMULATIONS OF RADIATION GENERATION FROM RELATIVISTIC ELECTRON BEAMS

AFOSR 88-0027

FINAL TECHNICAL REPORT

TO

AIR FORCE OFFICE OF SCIENTIFIC RESEARCH

Dr. Anthony T. Lin

Department of Physics
University of California, Los Angeles
Los Angeles, CA 90024-1547

October 1, 1989, to September 30, 1990

TABLE OF CONTENTS

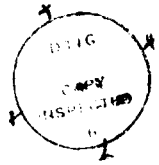

I. Introduction

This is the Final Technical Report on work performed under the support of the Air Force Office of Scientific Research under Grant AFOSR 88-0027 for the period October 1, 1989, to September 30, 1990. The objective of this work was to carry out basic physics research on the generation of coherent, tunable radiation from relativistic electron beams and exploring means of improving performances.

II. Summary of Work Accomplished

This work covered computer simulations and theoretical studies of radiation generation in three different free electron microwave devices: the cyclotron autoresonance maser (CARM), the backward wave oscillator (BWO), and the magnicon.

In investigating the effects of magnetic field on the output power of a plasma-filled Backward Wave Oscillator, we found that within a certain range of magnetic field the growth rate of beam-plasma cyclotron interaction is significantly larger than the conventional backward wave oscillation. This slow plasma cyclotron wave is emitted from plasmas only if it also satisfies the dispersion relation of a ripple wall waveguide which couples the slow wave to fast wave. This observation can be employed to more correctly interpret previous experiments carried out in the Soviet Unions which displayed a strong dependence of output power on the magnetic field.

We have carried out computer simulations of a 100 GHz electron cyclotron autoresonance maser oscillator that was designed for an experiment at the Naval Research Laboratory. The results indicate an intrinsically low efficiency for the experimental parameters. Enhancement of the efficiency by varying the beam current, interaction length, magnetic

field,and tapering the magnetic field are investigated. It is demonstrated that an efficiency above 20% may be obtained by reducing or tapering the magnetic field.

In simulating the performance of a Magnicon, we found that the saturation mechanism for the uniform magnetic field case is due to the phase detuning between the electron beam and electromagnetic wave. On the other hand, the conversion of electron kinetic energy to radiation in the tapered magnetic field case is terminated only if the electrons deplete their entire transverse energy.

A unifed theory is developed for free electron lasers, cyclotron autoresonance masers, and ion channel lasers. Based on this theory, parametric studies have been carried out to determine when different bunching mechanisms enhance or interfere with each other.

Below, we summarize the scope and main findings of these investigations. More detailed information are contained in the appended reports.

II.1 Emission of Plasma Cyclotron Waves in Plasma-Filled BWO

(Appendix 1)

Previously, there were two experiments in relativistic plasma-filled BWO which studied the dependence of output power on the magnetic field. Both results illustrated that the output power peaked at a certain magnetic field and they all conjectured that the resonance was due to $n\Omega_b = k_o V_o$. However, the experimental parameters used did not satisfy this resonance condition. Both experiments employed a small solid beam.

We have carried out computer simulations using the experimental parameters to elucidate the physics mechanism which gives rise to the

resonance behavior. A vacuum BWO simulations with $\Omega_b = 10\omega_c$ have been carried out. No instability (conventional BWO) has been observed for a solid beam with $R_b = 0.3R_o$ which was used in the early experiment. In the presence of the dense background plasma ($\omega_p = 0.45\omega_c$) and using $\Omega_p = 1.57\omega_c$, the slow plasma cyclotron wave is observed to be unstable. This wave is mainly supported by the background plasma and it can only leak out evanescently if no wave conversion mechanism is provided. The detector placed outside the plasma will be very difficult to observe this instability. By varying the magnetic field, the intersection between the beam slow space charge mode and the plasma cyclotron mode can be brought to coincide with the dispersion curve of the electromagnetic branch in a ripple waveguide. The excitation of the fast wave branch of the TM waveguide mode is observed only if Ω_p is in the neighborhood of $1.32\omega_c$. This result reproduces quite well the experimental curve which displays the output power versus magnetic field. The observed mechanism will have important implications in building a medium power beam-plasma microwave device which will be discussed in section III.1.

II.2 Cyclotron Autoresonance Maser Oscillator

(Appendix 2)

In a CARM amplifier an injection source is required which in some frequency region may not be readily available. Recently, attempts have been made at the Naval Reserach Laboratory to develop a 100GHz, 24MW CARM ocillator operating with 20% efficiency. Initial results show disappointingly low efficiency with mode competition suspected to be the cause.

The main findings for our simulation results are: Even in the absence of mode competition (priming) the efficiency at the experimental

parameters is very low, only about 3%. Higher efficiency may be achieved by either using a lower magnetic field or tapering the magnetic field. By tapering the magnetic field simulations using a higher beam current of 400 amps show it is possible to attain an efficiency above 20% for an electron beam with no velocity spread, and above 10% with the experimental anticipated maximum velocity spread of 3%.

No gyrotron mode competition was observed in any of the simulations. The efficiencies were thus, obtained under essentially ideal single-mode operation. The absence of gyrotron mode competition could be due to our priming the oscillator at the CARM frequency, which allows the CARM mode to start at a much higher power relative to the gyrotron mode (which has to start from the intitial noise). We find that without the priming, the initial broad band k_z-spectrum of the rf field from noise will evolve into two peaks centered at the CARM and gyrotron resonances, and the rf field takes a long time to grow. This confirms the possibility that priming could be beneficial in discriminating against unwanted longitudinal as well as transverse modes.

II.3 Magnicon

Most microwave free electron devices start with random phases between electrons and electromagnetic wave and rely on electron bunching to efficiently generate microwave radiation. On the other hand, there are generation mechanisms which require no electron bunching by injecting the electrons into the cavity with optimal single phase, such as the Magnicon which has recently been shown to produce 2.6MW output microwave pulse of 30μs at 0.915GHz with 85% efficiency. The output cavity works in the TM_{110} mode and the device operates on gyroresonance ($\omega_0 = \Omega$) without the Doppler shift term, and the electron entrance into the output resonator is

varied continuously in synchronism with the wave rotation. The energy conversion from electrons to the wave is determined from an approximate balance relation of the Lorentz forces between $eE_{||} = - e\omega r B_\perp$ and $ev_\perp B_\perp = e\omega r B_\perp$. Thus, during the wave-particle interaction, the electron transverse energy is converted into longitudinal energy and dissipated into $E_{||}$. The axial momentum should remain constant which implies that as the electron loses energy, its axial velocity increases.

We have developed a self-consistent large signal code to study the Magnicon interaction. The preliminary simulation results are shown in Fig. 1 and 2 using the TM_{110} mode, and the following parameters: $\alpha = v_\perp/v_{||} = 4$, $R_g/\rho_L = 1$, 300kV and 60 A beam (off-axis encircling beam). The interaction is optimized by varying the axial interaction length and tapering the axial magnetic field (B_0). The best result we attain so far uses $\nabla B_0/B_0 = 0.2/L$ (L = 44 cm). The time evolution of the electron transverse velocity in a wave field near the device axis and a resonant axial uniform magnetic field can be expressed as

$$V_\perp = \left(v_{\perp O}^2 + \Omega_{HF}^2 v_{ZO}^2 t^2 - 2\Omega_{HF} v_{zo} t \sin\phi \right)^{1/2} , \qquad (1)$$

where $\Phi = \kappa - \phi$, and κ is the electron entrance phase and ϕ is the rf phase. Equation (1) shows that when $\Phi = \pi/2$, $v_\perp$ decreases linearly in time, Figure 1 display the time evolution of the electron energy (γ_R) when it comes out of the cavity and the cavity field energy (W_f) which demonstrates that tapering the magnetic field increases the efficiency from 65% to 85%. Figure 2 shows the spatial evolution of the test electron energy and its phase relative to the wave (θ). In the simulation the electromagnetic wave grows from the background noise. For the untapered case, θ starts at around $\pi/2$ which is

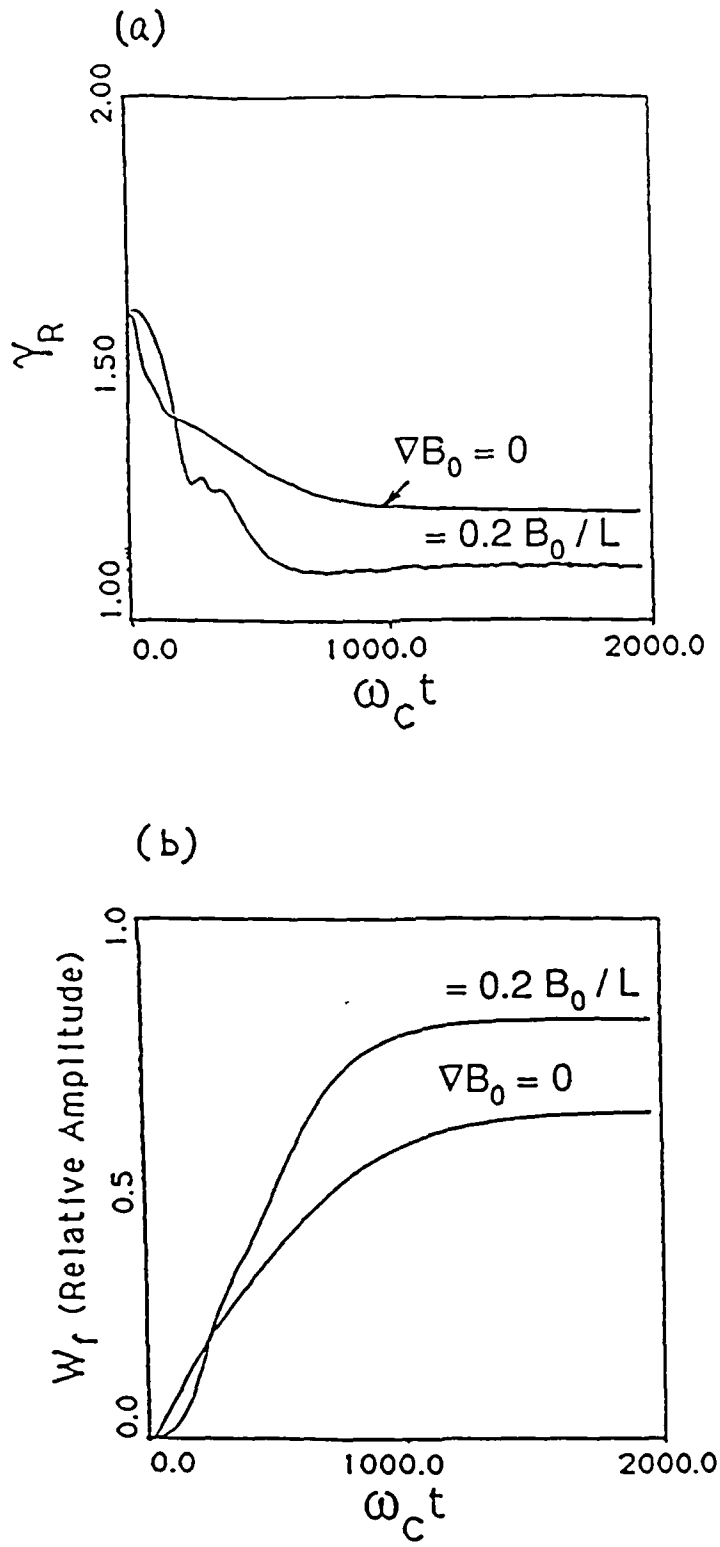

Comparison between tapered and untapered Magnicon. Time evolution of (a) electron energy at the exit plane, (b) resonator field energy.

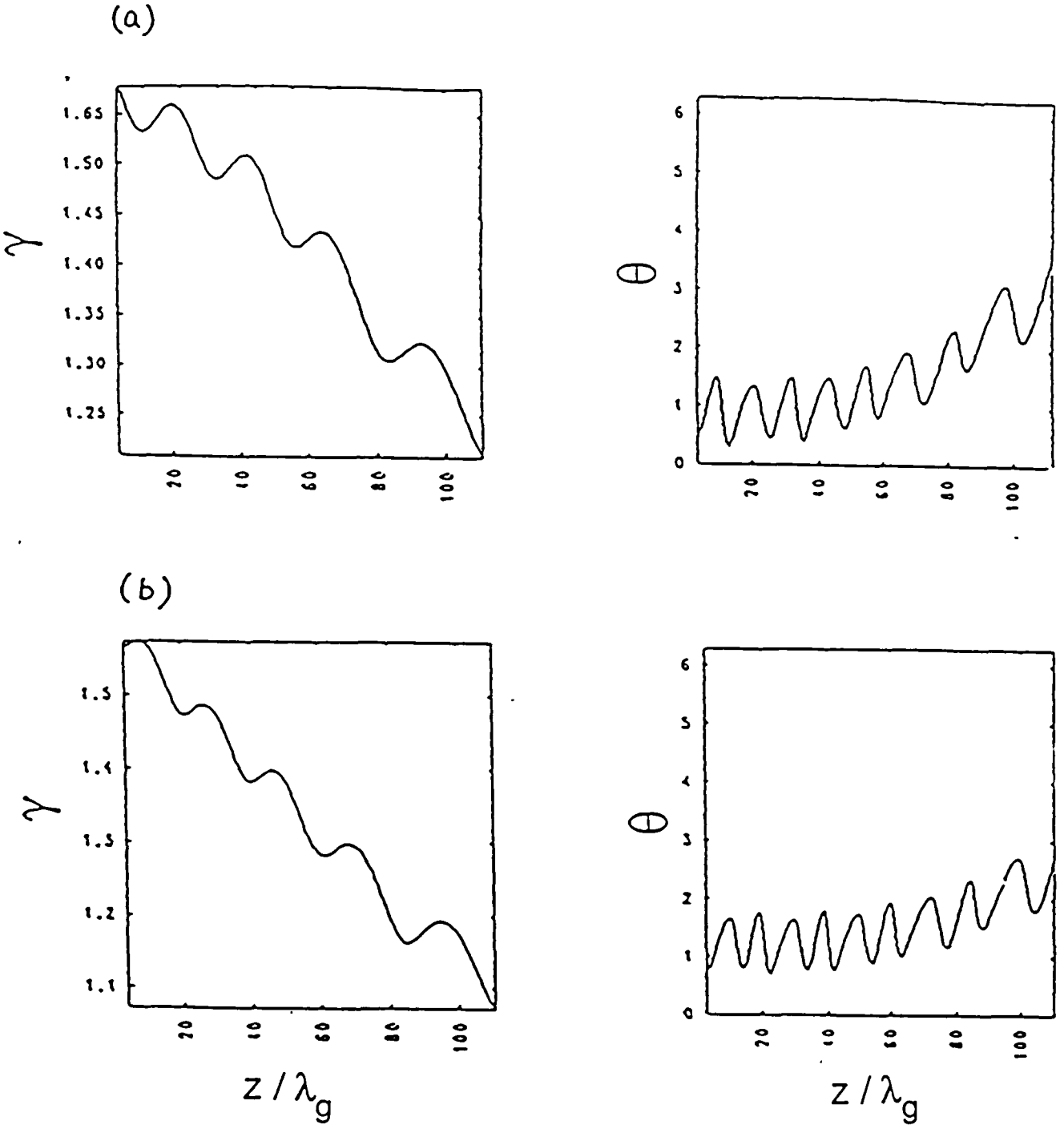

The energy and phase spatial variation (λ_g = 0.4 cm) of a test electron for (a) $\nabla B_o = 0$, and (b) $\nabla B_o = 0.2\ B_o/L$.

the optional entrance phase (Eq. 1) and becomes about π when the conversion process terminates ($\vec{V}_\perp \times \vec{B}_\perp = 0$). The change in θ is primarily due to the increase in the electron relativistic cyclotron frequency as it loses energy. This detuning can be compensated by tapering the magnetic field. In this case the conversion process ends when the electron transverse energy vanishes. Although the electron starts with 93% of its energy residing along the transverse direction, the optimized efficiency reaches only 85%. This is because during the conversion process $P_{||} = m_o \gamma V_{||}$ remains constant. As γ decreases $V_{||}$ has to increase. We continue investigating the Magnicon and the investigation will be extended to include the harmonic Magicon.

II.4 Unified Theory for CARM, ICL, and FEL

(Appendix 3)

Recently, a new radiation source, the Ion-Channel Laser (ICL) was conceived at UCLA. In this device, a relativistic electron beam is injected into an underdense plasma ($\omega_p < \omega_b$). The beam front pushes out the plasma electrons leaving an ion channel. The ion focusing force causes the beam electrons to oscillate about the axis and plays a similar role as the magnetic field in a CARM. Radiation can be generated ranged from microwaves to soft-X-rays.

We have developed a unified theory to describe the amplification mechanism for CARM, ICL, and FEL. The theory assumes that the dependence of electron gyrofrequency on its beam energy is in the form of γ^{-q} where q = 1, $\frac{1}{2}$, and 0, respectively for CARM, ICL, and FEL. The main findings are : Azimuthal bunching dominates over axial bunching if q(1-

$v_{oz}/v_{ph}) > (\frac{c^2}{v_{ph}^2} - \frac{v_{oz}}{v_{ph}})$ and vice versa. If $v_{oz} > v_{ph}$ or $c^2 < v_{oz}\, v_{ph}$, the two bunchings reinforce each other rather than offsetting which gives rise to no autoresonance. In order to have wave amplification, the sign of mismatch has to be the same as the sign of bunching parameter. For CARMs and ICLs the relativistic mass variation effect on the electron axial velocity may overwhelm the $\vec{v} \times \vec{B}$ force so that the chan' in axial veloicty is opposite to the electron energy change and the axial bunching term becomes negative. For FELs the bunching arising from the relativistic mass variation is smaller than that of the ponderomotive force induced by the wiggler and the wave so the FEL bunching paramerer is always negative. All these devices can upshift the electron undulation frequency by a factor of $2\gamma_{oz}^2$.

References:

1. M.M. Karliner, et al., Nuclear Instruments and Methods in Phys. Research, A269, 459 (1988).

III. AFOSR Supported Publications (October 1, 1989-September 30, 1990)

1. A.T. Lin and Chih-Chien Lin, "Stabilization of the Absolute Instability in Cyclotron Autoresonance Maser Amplifiers by a Drive Wave", Phys. Fluids B, 1, 2286 (1989).

2. A.T. Lin and L. Chen, "Plasma - Induced Efficiency Enhancement in a Backward Wave Oscillator", Phys. Rev. Letts, 63, 2808 (1989).

3. T.H. Kho and A.T. Lin, "Efficiency Dependence on Beam Current and Input Power in a Cyclotron Autoresonance Maser Amplifier," Phys. Fluids B, 2, 822 (1990).

4. T.H. Kho and A.T Lin, " Cyclotron - Cherenkov and Cherenkov Instabilities," Special Issue on High Power Microwave Generation", IEEE Trans-Plasma Science, 18, 513 (1990).

5. T.H. Kho and A.T. Lin, "Computer Simulations of A 100 GHz CARM Oscillator with Bragg Reflectors", to appear in Nuclear Instruments and Methods in Phys. Research (1990).

6. A.T. Lin, "Emission of Plasma Cyclotron Waves in Plasma-Filled Backward Wave Oscillators", Phys. Rev. Lett., 65, 717 (1990).

7. K.R. Chen, J. M. Dawson, A.T. Lin and T. Katsouleas, "Unifed Theory and Comparative Study of CARMs, ICLs, and FELs," submitted to Phys. Fluids B., (1990).

APPENDICES

1. Emission of Plasma Cyclotron Waves in Plasma-Filled Backward-Wave Oscillators.
2. Computer Simulations of a 100 GHz Cyclotron Autoresonance Maser Oscillator with Bragg Reflectors.
3. Unified Theory and Comparative Study of CARMs, ICLs and FELs.

APPENDIX 1

Emission of Plasma Cyclotron Waves in Plasma-Filled Backward-Wave Oscillators

A. T. Lin

Department of Physics, University of California, Los Angeles, California 90024-1547

(Received 27 February 1990)

It is found through computer simulations of plasma-filled backward-wave oscillators that within a certain range of magnetic field the growth rate of beam-plasma cyclotron interaction is significantly larger than the conventional backward-wave oscillation. This slow plasma cyclotron wave is emitted from plasmas only if it also satisfies the dispersion relation of a rippled-wall waveguide which couples the slow wave to fast wave. This observation may be employed to interpret previous experiments which displayed a strong dependence of output power on the magnetic field.

PACS numbers: 52.60.+h, 52.65.+z

Recently, a considerable amount of effort[1-5] has been undertaken towards the production of ultrahigh-power microwave sources based on backward-wave oscillator (BWO) configurations, in which a rippled-wall slow-wave structure provides a very efficient way of converting the kinetic energy of relativistic electron beams into microwave radiations.

In order to raise the relativistic beam current and hence the output power of relativistic electronic devices, a background plasma is sometimes employed to provide space-charge neutralization. The plasma may also induce some other effects which could influence the outcome of backward-wave oscillators. Experimentally, it has been observed[6] that the efficiency can be increased by a factor of 8 when the plasma frequency $\omega_p \simeq 0.2ck_0$ (k_0 is the rippled-wall wave number and c is the speed of light) and the enhancement mechanism was attributed to the excitation of beam-plasma backward-wave instability. Very recently, computer-simulation results[7] have demonstrated that a more plausible explanation for the efficiency enhancement is that a dense background plasma tends to reduce the phase velocity of the most unstable mode in a BWO and causes the beam to convert more energy to the wave.

The investigations described above all impose a strong magnetic field to confine the electron motion to only one dimension. In vacuum BWO's,[8] the output powers were observed to depend on the magnetic field. The beam cyclotron resonance absorbed the BWO emission and introduced a dip in the curve of the output power versus the magnetic field. This issue will not be treated in this paper. On the other hand, experiments[9] in relativistic plasma-filled BWO illustrated that the output power peaked at a certain magnetic field and they conjectured that the resonance was due to $n\Omega_b = k_0 V_0$ (Ω_b is the relativistic beam cyclotron frequency, n is the harmonic number, and V_0 is the beam axial velocity). However, the experimental parameters used did not satisfy this resonance condition. In this paper we will demonstrate through computer simulations that the excitation of slow plasma cyclotron waves when they also satisfy the dispersion relation of a rippled-wall waveguide can give rise to the resonance characteristics observed in the experiment. This mechanism can be utilized to convert the slow wave into fast wave, and thus overcome one of the major obstacles in realizing beam-plasma interaction, to build a compact medium-power microwave device.

The dispersion characteristics of a plasma-filled rippled-wall waveguide [$R_w = R_0(1+\varepsilon \sin k_0 z)$, ε is the ripple depth] immersed in an infinite magnetic field have previously been shown[6] and confirmed by our particle simulations. They consist of the electromagnetic branch of the rippled-wall waveguide and a plasma-wave branch. The effect of a finite magnetic field introduces a plasma cyclotron wave branch. The dispersion relation of the plasma-wave branches in a plasma-filled waveguide is expressed by[10]

$$\left(\frac{kc}{\omega_c}\right)^2 = -\frac{1+\omega_p^2/(\Omega_p^2-\omega^2)}{1-\omega_p^2/\omega^2}, \tag{1}$$

where ω_c is the waveguide cutoff frequency, ω_p is the plasma frequency, and Ω_p is the plasma cyclotron frequency. In the case of $\Omega_p > \omega_p$, the uncoupled dispersion relations are shown in Fig. 1(a). Notice that in this situation, the frequency of the plasma cyclotron wave branch can be higher than the cutoff frequency of a plasma-filled waveguide, whereas the plasma-wave branch is always lower. A finite magnetic field will also introduce the cyclotron resonance lines associated with the relativistic electron beam [$\omega = kV_0 \pm \Omega_b$, Fig. 1(a)]. The excitation of the fast cyclotron wave[11] ($+\Omega_b$) demands a certain amount of beam initial transverse momentum, whereas the slow cyclotron wave[12] ($-\Omega_b$) requires a slow-wave structure.

In order to address the finite-magnetic-field effects on the plasma-filled BWO output power, a particle waveguide code whose algorithms have been described previously[7] is used. Transversely, only the TM_{01} mode is retained while periodic boundary conditions are imposed along the axial direction so that the nth mode wave number is defined as $k_{zn} = 2\pi n/L$, where L is the system length and is taken to be $256\lambda_g$ (λ_g is the spatial grid size). To take into account the coupling of the TE_{01} and the TM_{01} modes through electron gyration, simulations which included both modes were also carried out. The results only differed by a few percent from the single-

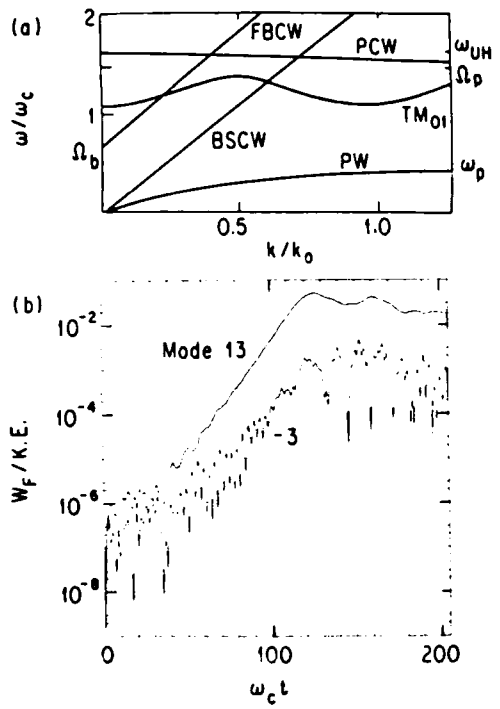

FIG. 1. The propagation characteristics of a plasma-filled rippled waveguide: (a) the dispersion relation with a finite magnetic field. (PW, plasma wave; PCW, plasma cyclotron wave; BSCW, beam space-charge wave; FBCW, fast-beam cyclotron wave.) (b) The time evolution of wave energy of unstable modes ($\Omega_p = 1.57\omega_c$).

mode simulation. To facilitate the comparison between experimental and simulation results, the experimental parameters[8] were used in our simulation. The beam energy and current are respectively 700 kV and 4 kA. The rippled-wall waveguide dimensions are the following: $R_0 = 13.9\lambda_g$, $\lambda_g = 0.1$ cm, $\varepsilon = 0.1$, and $k_0 = k_{zn}$ for $n = 16$ in our simulation system. Plasma electrons are assumed to fill up uniformly the waveguide cross section up to $R = R_0(1-\varepsilon)$ and $R = 0.3R_0$ for beam electrons. All frequencies are normalized to ω_c. The plasma density can be varied and it will affect the location where the output power is peaked with respect to the magnetic field. The following simulation results are for $\omega_p = 0.45\omega_c$. Simulations using $R_0 = 22.5\lambda_g$ were also carried out. The resonance behavior of the output power versus the magnetic field remains the same.

Consider a solid beam without any initial transverse momentum. The conventional beam-forward plasma-wave instability can be avoided if $\omega_p/\omega_c < \gamma_0 V_0/c$ (γ_0 is the beam relativistic factor), which is satisfied in our simulation. The BWO instability (surface wave) is most effective when a hollow beam placed very close to the waveguide wall is employed. A vacuum BWO simulation with $\Omega_b = 10\omega_c$ was carried out. A very weak instability was observed for a solid beam with $R_b = 0.3R_0$ which was used in the early experiment.[9] No significant growth was observed over the time of the simulation run. As was demonstrated in our early work,[7] using a large radius beam, the growth rate estimated from the simulation result agrees quite well with the theoretical prediction. In the presence of the dense background plasma and using $\Omega_p = 1.57\omega_c$, the time evolutions of the most unstable wave energy are shown in Fig. 1(b). The growth rate estimated from simulation results is $\omega_i = 0.058\omega_c$, which is rather strong because it is a volume-wave interaction. However, this slow plasma cyclotron wave is mainly supported by the background plasma and it can only leak out evanescently if no wave conversion mechanism is provided. With the detector placed outside the plasma it would be very difficult to observe this instability. The frequency spectrum of the unstable mode ($n = 13$) peaks at $\omega = 1.62\omega_c$, which falls on the dispersion curve of the plasma cyclotron wave. In this case, the fast-electromagnetic-wave component ($n = -3$) is relatively small in comparison with the plasma cyclotron wave.

By varying the magnetic field, the intersection between the beam slow space-charge mode and the plasma cyclotron mode can be brought to coincidence with the dispersion curve of the electromagnetic branch in a rippled-wall waveguide. In conventional BWO interactions, the resonance conditions $\{\omega = kV_0 - \omega_b/\gamma_0^{3/2}$ and $\omega = [\omega_c^2 + (k-k_0)^2c^2]^{1/2}\}$ are usually satisfied simultaneously. These expressions indicate that the slow space-charge beam mode in the zeroth-order Brillouin zone should be coupled with the TM waveguide mode in the first-order Brillouin zone and grow together with the same growth rate. To illustrate the magnetic-field resonance effect, a series of simulations using different magnetic-field strengths have been carried out and the results are displayed in Fig. 2. The excitation of the fast-wave branch of the TM waveguide mode is observed only if Ω_p is in the neighborhood of $1.32\omega_c$. The wave energy time evolutions of the plasma cyclotron mode ($n = 11$) and the fast electromagnetic-wave mode ($n = -5$) are shown in Fig. 2(a). Their growth rate and real frequency are respectively $\omega_i = 0.065\omega_c$ and $\omega_r = 1.315\omega_c$. The peak efficiency of the interaction has achieved about 17%. In this case, the fast-electromagnetic-wave component ($n = -5$) is significantly larger than the plasma cyclotron wave. Since the plasma electrons participate actively in supporting the excitation of the plasma cyclotron wave, the saturation mechanism will involve the trapping of a portion of plasma electrons by the axial electric field of the excited slow wave. This has been demonstrated in Figs. 2(b) and 2(c), which plot the electron axial velocity versus distance at $\omega_c t = 0$ and at the time of saturation ($\omega_c t = 140$), which clearly illustrates the active participation of plasma electrons in the formation of trapped structures. In doing so, the plasma electrons gain significant amounts of kinetic energy at the expense of beam energy and thus reduce the overall efficiency in microwave generation. Figure 3(a) shows the time evolution of the beam and the plasma kinetic energy. At the time of saturation, the beam electrons

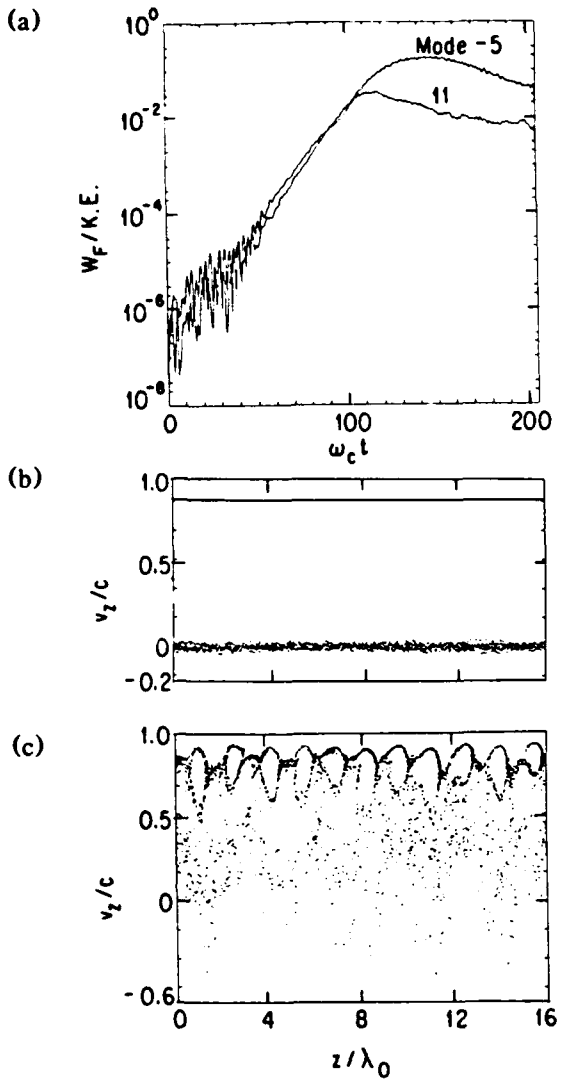

FIG. 2. Simulation results of a plasma-filled BWO ($\Omega_p = 1.32\omega_c$): (a) The time evolution of wave energy of unstable modes; electron axial velocity vs distance at (b) $\omega_c t = 0$ and (c) $\omega_c t = 140$.

have on the average lost 30% of their kinetic energy. However, almost half of it is spent in increasing the plasma kinetic energy. In comparison with a conventional BWO, this could constitute a disadvantage of constructing microwave tubes based on the excitation of plasma waves. The wave energy versus magnetic field is plotted in Fig. 3(b). The results clearly reveal pronounced peak at $\Omega_p = 1.32\omega_c$. Furthermore, the simulation results also show that for the absence of the background plasma the peak no longer exists. In the resonance region ($\Omega_p = 1.25\omega_c - 1.4\omega_c$), the output frequency from simulations remains relatively constant ($\omega_r = 1.315\omega_c$). This is due to the fact that the plasma cyclotron wave-dispersion curve is modified when the unstable mode is also a normal mode of the rippled-wall waveguide. Outside the resonance region, the unstable mode frequency follows the plasma cyclotron wave-dispersion relation. However, in these cases, the wave energy is mostly dominated by the slow wave and saturated at low levels.

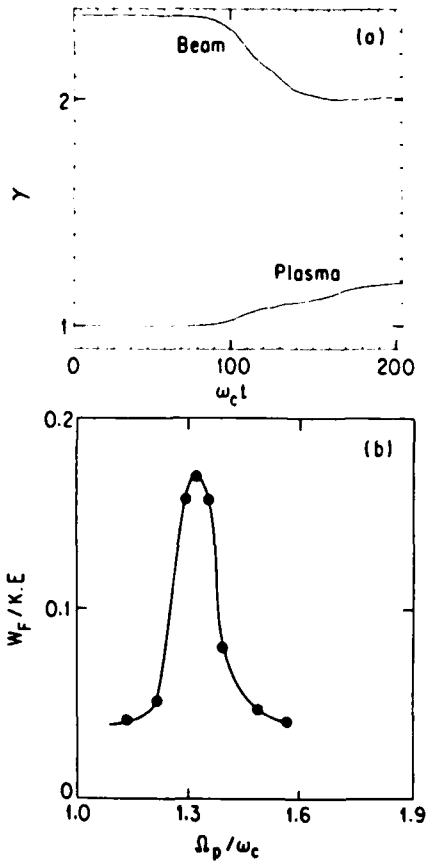

FIG. 3. Simulation results: (a) The time evolution of beam and plasma energy ($\Omega_p = 1.32\omega_c$); (b) the emitted energy vs magnetic field.

Based on the fact that the emission can be detected only if a fast wave is generated, the experimentally observed radiation outside the resonance region[9] was dominated by the weakly growing vacuum BWO instability. This can explain why the output frequency measured in the experiment is independent of the magnetic field.

These findings may be used to interpret previous experimental results which showed that the emission was peaked at $B_0 = 3.85$ kG and $\beta_\perp = 0.3$ ($\beta_\perp = v_\perp/c$). They attributed that in addition to the conventional BWO resonances, the fast-beam cyclotron resonance is also satisfied [$\omega = (k - k_0)V_0 + n\Omega_b$]. They claimed that if $k_0 V_0 = n\Omega_b$, the fast-beam cyclotron resonance becomes $\omega = kV_0$. Therefore, all three resonances are satisfied simultaneously, which then give rise to the resonance behavior of the emission power versus magnetic field. Although the background plasma density was as high as 10^{12} cm^{-3}, they believed that plasma only provided the space-charge neutralization. However, experimental parameters give $k_0 V_0 = 3.54\Omega_b$ while the observed microwave frequency is very close to the plasma cyclotron frequency. To satisfy their resonance condition, coupling to higher harmonics of k_0 and Ω_b are required, which is unlikely. On the other hand, Fig. 1(a) indicates that with sufficient initial transverse momentum the fast-beam cyclotron mode should be able to excite the fast-

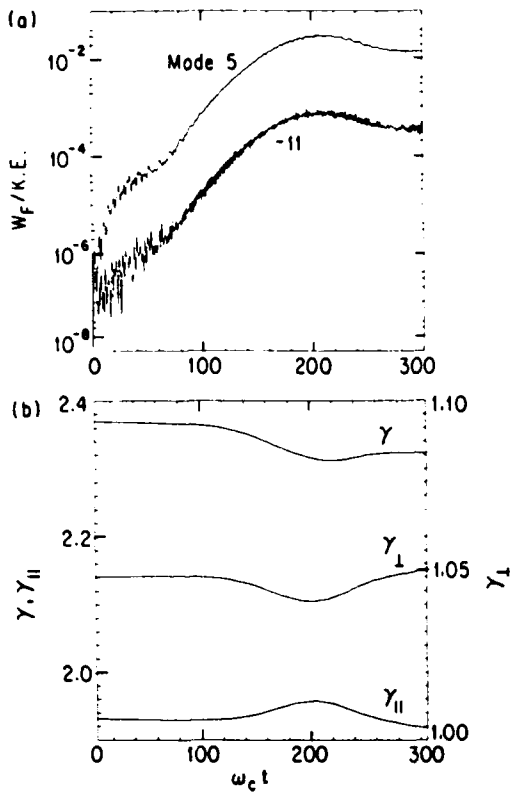

FIG. 4. Fast-beam cyclotron wave instability ($\Omega_b = 0.66\omega_c$): (a) The time evolution of wave energy of most unstable modes; (b) the time evolution of beam kinetic energy.

wave branch of the TM waveguide mode. To illustrate this interaction, a simulation run using $\beta_\perp = 0.3$, $\Omega_b = 0.66\omega_c$, and without background plasma was carried out. The wave energy time evolutions of the most unstable modes are shown in Fig. 4(a). The excited waves exponentiate at the growth rate of $\omega_i = 0.029\omega_c$, which is weaker than the plasma cyclotron wave instability and oscillate at $\omega_r = 1.3\omega_c$, which satisfies the fast-beam cyclotron wave-dispersion relation ($\omega = kV_0 + \Omega_b$). The saturation efficiency attained about 3%. Figure 4(b) plots the time evolutions of beam transverse and longitudinal energies which demonstrate that the instability only depletes the transverse component of beam energy. This energy depletion characteristic further supports that the interaction is not due to the vacuum BWO mechanism.

As is evident from computer simulations, the excitation of plasma cyclotron waves requires no initial beam transverse momentum. To reconcile the experimental observation that the emission was peaked at $\beta_\perp = 0.3$, a series of simulations varying $\beta_\perp$ has been carried out. The change in $\beta_\perp$ results in a change in the slope of the slow space-charge wave resonance line (V_0) and consequently affects the resonance magnetic field. The simulation results show that the emission is peaked at $\beta_\perp = 0.2$. The increase in efficiency from $\beta_\perp = 0$ to $\beta_\perp = 0.2$ is relatively mild but the decrease from $\beta_\perp = 0.2$ to $\beta_\perp = 0.3$ is more drastic. The emission is now peaked at $\Omega_p = 1.26\omega_c$ for $\beta_\perp = 0.2$ and the fast-beam cyclotron instability is overwhelmed by the plasma cyclotron instability. In any event, the accuracy that the $\beta_\perp$ measurement can attain is unknown and so the dependence of the emission on $\beta_\perp$ will not be pursued further.

In conclusion, through computer simulations plasma cyclotron waves are observed to be readily excited by the relativistic electron beam propagating in a plasma-filled BWO. When the excited mode also coincides with the electromagnetic-wave-dispersion relation of a rippled-wall waveguide, the slow plasma cyclotron wave is efficiently converted into a fast wave through the rippled-wall boundary and can be easily detected outside the plasma. This mechanism can be utilized to explain the early experimental results which displayed strong dependence of the emitted power on magnetic field from a plasma-filled BWO. Because of its high gain, the observed mechanism can be employed to build compact microwave tubes with medium beam energy of the order of 100 kW. The limitation that the observed instability will impose on the plasma-filled gyrotron should also be investigated.

This work was supported by the Air Force Office of Scientific Research under Grant No. AFOSR 88-0027 and the San Diego Supercomputing Center.

[1]Y. Carmel, J. Ivers, R. E. Kribel, and J. Nation, Phys. Rev. Lett. **33**, 1278 (1974).

[2]V. L. Bratman *et al.*, Pis'ma Zh. Tekh. Fiz. **9**, 617 (1983) [Sov. Tech. Lett. **9**, 266 (1983)].

[3]Y. Carmel, V. L. Granatstein, and A. Gover, Phys. Rev. Lett. **51**, 566 (1983).

[4]A. Bromborsky and B. Ruth, IEEE Trans. Microwave Theory Tech. **32**, 600 (1984).

[5]J. A. Swegle, J. W. Poukey, and G. T. Leifeste, Phys. Fluids **28**, 2882 (1985).

[6]Y. Carmel *et al.*, Phys. Rev. Lett. **62**, 2389 (1989).

[7]A. T. Lin and L. Chen, Phys. Rev. Lett. **63**, 2808 (1989).

[8]N. M. Bykov *et al.*, Zh. Tekh. Fiz. **59**, 32 (1989) [Sov. Phys. Tech. Phys. **34**, 519 (1989)].

[9]Y. V. Tkach *et al.*, Fiz. Plazmy **5**, 566 (1979) [Sov. J. Plasma Phys. **5**, 566 (1979)].

[10]N. A. Krall and A. W. Trivelpiece, *Principles of Plasma Physics* (San Francisco, San Francisco, 1986), Chap. 4.

[11]A. T. Lin, Int. J. Electron. **57**, 1097 (1984).

[12]T. H. Kho and A. T. Lin, Phys. Rev. A **38**, 2883 (1988).

APPENDIX 2

COMPUTER SIMULATIONS OF A 100 GHz CYCLOTRON AUTORESONANCE MASER OSCILLATOR WITH BRAGG REFLECTORS

T.H. Kho and A.T. Lin

Physics Dept., University of California at Los Angeles

Los Angeles, CA 90024

Abstract

Computer simulations of a 100 GHz electron cyclotron autoresonance maser (CARM) oscillator that has been designed for an experiment at the Naval Research Laboratory are carried out using a time-dependent, 3-D, particle-in-cell code. The results indicate an intrinsically low efficiency for the experimental parameters. Enhancement of the efficiency by varying the beam current, interaction length, magnetic field, and tapering the magnetic field are investigated. It is demonstrated that an efficiency above 20% may be obtained by reducing or tapering the magnetic field.

Theoretical and numerical studies of the electron cyclotron autoresonance maser (CARM) indicate that it poses a strong alternative to the free electron laser as a high power, high efficiency radiation source in the millimeter to submillimeter wavelengths [1-5]. However, there have been few CARM experiments to date and the potential high efficiency of the CARM has yet to be demonstrated in the laboratory. The first CARM experiments [6,7] achieved only 2-4% efficiency. More recently, attempts have been made at the Naval Research Laboratory [8] to develop a 100 GHz, 24 MW CARM oscillator operating with 20% efficiency. Initial results show disappointingly low efficiency of only a few percent, with mode competition suspected to be the cause [9].

We have developed a 3-D, time-dependent, particle-in-cell code to model a CARM oscillator with the same configuration as the NRL experiment and carried out simulations for similar beam parameters. The parameters of the NRL experiment are shown in Table 1. The CARM oscillator consists of a cylindrical waveguide with a smooth-wall central section connected on either side to rippled-wall sections, or Bragg reflectors. The ripple period is half the wavelength of the desired cavity mode so that the latter is strongly reflected. The virtue of this Bragg cavity is that it confines the radiation while allowing unimpeded passage to the electron beam.

For the parameters in Table 1, the cyclotron beam line intersects the vacuum TE_{61} mode at two frequencies, as shown in Fig. 1; the higher frequency is the desired CARM operation, and the lower frequency corresponds to the gyrotron interaction. The simulations here include multiple longitudinal modes but only one transverse waveguide mode, the anticipated TE_{61} mode. Thus, mode competition between the TE_{61} gyrotron and CARM modes is included self-consistently but mode competition between different transverse modes is not considered.

In this paper, we describe the numerical model and present results from the simulations. The main findings are: Even in the absence of mode competition the efficiency at the experimental parameters is very low, only about 3%. Higher efficiency may be achieved by either using a lower magnetic field or tapering the magnetic field. By tapering the magnetic field, simulations using a higher beam current of 400 amps show it is possible to achieve an efficiency above 20% for an electron beam with no velocity spread, and above 10% with the anticipated maximum velocity spread of 3%.

We briefly describe here the numerical algorithm used in modeling the CARM oscillator. This numerical algorithm has used successfully in the past to model gyrotrons, and further details may be found in Refs. [10-12]. In the open waveguide structure of the Bragg cavity, the transverse dependence of the fields at every position z along the axis can be expanded into a complete set of the local orthogonal transverse electric and magnetic modes of the empty waveguide. For simplicity, however, we assume that the desired TE_{61} mode is the dominant mode and the fields are well represented by retaining only that mode in the expansion. For a given TE_{mn} mode, the electric and magnetic fields may be written as

$$\underline{E}_{mn} = \sum_{p=1,2} E^{p}_{Tmn}(z,t)(\hat{\underline{z}} \times \nabla_{\perp} C^{p}_{mn}) \tag{1a}$$

$$\underline{B}_{mn} = -\sum_{p=1,2} B^{p}_{Tmn}(z,t)\nabla_{\perp} C^{p}_{mn} + \hat{\underline{z}}\, B^{p}_{Lmn} k_{mn} C^{p}_{mn} \tag{1b}$$

where C^{p}_{mn} is the local wave function with polarization p, given by

$$C^{1,2}_{mn} = -\frac{2r_W}{k_{mn}} J_m(k_{mn} r/a(z)) \begin{Bmatrix} Cos(m\theta) \\ Sin(m\theta) \end{Bmatrix} \tag{2}$$

Here, r_w and a(z) are the mean and local wall radii, respectively, and J_m is the mth order Bessel function, and k_{mn} the nth root of $J'_m(k_{mn}) = 0$. The wall radius can be an arbitrary continuous function of axial position, allowing the nonuniform cavity wall of the oscillator to be modeled.

Neglecting the effects of mode conversion through changes in the local cavity radius, the time evolution of the rf fields from Maxwell's equations is given by

$$\frac{\partial E^p_{Tmn}}{\partial t} = -c\frac{\partial B^p_{Tmn}}{\partial t} + \omega_{mn}(z)B^p_{Lmn} - cB^p_{Tmn}\frac{a'}{a}\left(\frac{m^2}{k^2_{mn} - m^2}\right) - \frac{2L_p}{N_p}\left(\frac{\omega_B}{\omega_{co}}\right)^2\frac{r_w}{U_{mn}a(z)}\sum_j\left[V_{xj}e^p_{xmn}(x_j,y_j) + V_{yj}e^p_{ymn}(x_j,y_j)\right] \quad (3a)$$

$$\frac{\partial B^p_{Tmn}}{\partial t} = -c\frac{\partial E^p_{Tmn}}{\partial t} + cE^p_{Tmn}\frac{a'}{a}\left(\frac{m^2}{k^2_{mn} - m^2}\right) \quad (3b)$$

$$\frac{\partial B^p_{Lmn}}{\partial t} = -\omega_{cmn}(z)E^p_{Tmn} \quad (3c)$$

where $\omega_{cmn}(z) = ck_{mn}/a(z)$ is the local waveguide cutoff frequency,

$$U_{mn} = J^2_m(k_{mn})\left(1-m^2/k^2_{mn}\right),$$

$$\left(\frac{\omega_B}{\omega_{co}}\right)^2 = \frac{5.875\times10^{-5}}{k^2_{mn}\beta_{zo}}I_b,$$

I_b being the total beam current in amperes.

The electron beam is modeled by thousands of macroelectrons whose trajectories are followed in time and space through the relativistic

equations of motion under the influence of the rf and externally applied magnetic fields:

$$\frac{d\underline{P}_j}{dt} = q_j\left[\underline{E}(\underline{r}_j) + \underline{V}_j \times \underline{B}(\underline{r}_j)/c\right], \tag{4a}$$

$$\frac{d\underline{r}_j}{dt} = \underline{V}_j. \tag{4b}$$

The updated macroelectron velocity and position are then used to evaluate the source current for the the rf fields (Eq.3a). In order to avoid the singularity at the cavity axis in advancing the electron trajectories, the calculations are carried out using Cartesian coordinates. The x and y components of the transverse field functions e^{P}_{xmn} and e^{P}_{ymn} are given by

$$e^{1,2}_{xmn} = \mp\left[J_{m-1}(k_{mn}r/a)\begin{Bmatrix}Sin(m-1)\theta\\Cos(m-1)\theta\end{Bmatrix} + J_{m+1}(k_{mn}r/a)\begin{Bmatrix}Sin(m+1)\theta\\Cos(m+1)\theta\end{Bmatrix}\right],$$

$$e^{1,2}_{ymn} = -\left[J_{m-1}(k_{mn}r/a)\begin{Bmatrix}Cos(m-1)\theta\\Sin(m-1)\theta\end{Bmatrix} - J_{m+1}(k_{mn}r/a)\begin{Bmatrix}Cos(m+1)\theta\\Sin(m+1)\theta\end{Bmatrix}\right].$$

The longitudinal dependence of the rf field is represented by a Fourier series expansion. Outside the cavity region, the em waves are numerically absorbed. The polarization of the modes is determined self-consistently in the simulation through interaction with the electron beam

The ripples of the Bragg reflectors are assumed to be sinusoidal with the periodicity and amplitudes given in Table 1. The reflectivities of the Bragg reflectors determined numerically by placing a 100 GHz, TE_{61} antenna a distance away from each reflector in an empty waveguide are 99% for the upstream and 89% for the downstream reflectors, in good agreement with the

theoretical predictions.

In the simulations, the beam electrons are continuously injected into the input end of the cavity with prescribed parameters, and removed at the output of the cavity; the input beam voltage is constant. An annular electron beam is assumed, with guiding center located at $0.8r_w$ in order to maximize the coupling between electrons and the TE_{61} waveguide mode.

The initial rf field in the cavity arises from numerical noise in the electron beam. However, in order to limit the computational time required to follow the oscillation to a steady state to a managable value, we also prime the oscillator by injecting an rf signal into the cavity for a short period of time along with the electron beam. In all the simulations presented below, a 100 GHz, ~ 200 kW wave was injected into the cavity for ~0.8 to ~1.8 ns to initiate the CARM interaction. Also, except for the results in Table 6, the electron beam has no velocity spread in the simulations; all other parameters are as given in Table 1, unless where otherwise specified.

Figure 2a illustrates a cross-sectional view of the electron beam in the cavity, and 2b, electron energies along the axis of the cavity. The electrons are injected at the entrance to the Bragg cavity, $z = 0$, and removed at the exit, $z = 7.1$ cm. Figure 3a shows an example of the electric field profile in the cavity, 3b the time history of the rf field energy, and 2c, energy of the spent electron beam as a function of time. The time taken to reach saturation is about 25 ns. The initial sharp rise in rf field energy in Fig. 3b (and the initial drop in Fig. 3c) is due to the injected signal. The efficiency reached is only about 3%. The efficiency, η, is defined as $\eta = (\gamma_o-\gamma_s)/(\gamma_o-1)$ where γ_o and γ_s are the initial and spent electron beam Lorentz factors.

We carried out a parameter search for better efficiency. Table 2 shows the efficiency and the (exponential) growth rate of the rf field energy in the cavity as a function of beam current, and Table 3, as a function of cavity length (changing only the length of the smooth section). None of these variation has much impact on the efficiency, although increasing the current, or cavity length, increases the growth rate as would be expected.

However, the efficiency could be increased significantly by tapering, or detuning (reducing) the magnetic field. Since tapering or detuning generally increases the time taken to reach a steady state, the following studies were carried out using an electron beam current of 400 A instead of 200 A, and thus, a higher growrh rate, in order to make the simulation more tractable. Table 4 shows the efficiency when the external magnetic field is uniformly reduced, and Table 5 shows the efficiency as a function of the tapered magnetic field. The magnetic field is tapered by reducing it linearly from $z = 0.0$ to $z = 7.1$ cm; in Table 5, $\Delta B/B_o = (B(z=7.1\text{cm}) - B(z=0.0))/B(z=0.0)$. It is seen that it is possible to achieve efficiencies somewhat above 20%. The sharp drop in efficiency in Table 4, from 21.5% to 0% over 1 kG is consistent with previous simulation results of magnetic field detuning [13]; although the efficiency increases as the magnetic field is decreased, the growth rate decreases and eventually vanishes. Note that changing the magnetic field would change the frequency in a superradiant CARM amplifier but in this oscillator, the operating frequency is fixed by the periodicity of the Bragg reflectors and is not affected by the magnetic field; thus, one still obtains 100 GHz radiation at the higher efficieny although the cyclotron resonance beam line has shifted.

Table 5 shows the effect of having axial velocity spreads of 1% and 3% (but with no energy spread) on the best case of 23% efficiency obtained by

tapering the magnetic field. A 1% spread reduces the growth rate somewhat but has no effect on the final efficiency. With the anticipated maximum velocity spread of 3%, the efficiency drops to 11%. Thus, with a 400 A electron beam, one might still be able to achieve above 20MW of power within the anticipated range of velocity spread.

No gyrotron mode competition was observed in any of the above simulations. The efficiencies were thus, obtained under essentially ideal single-mode operation. The absence of gyrotron mode competition could be due to our priming the oscillator at the CARM frequency, which allows the CARM mode to start at a much higher power relative to the gyrotron mode (which has to start from the initial noise). We find that without the priming, the initial broad band k_z- spectrum of the rf field from noise will evolve into two peaks centered at the CARM and gyrotron resonances, and the rf field takes a long time to grow. When the simulation is repeated with an artificial k_z-dependent resisitivity to suppress the gyrotron mode, the growth of the rf field is found to be enhanced which suggests that the the delay in oscillation is due to mode competition. However, one should be cautious about extrapolating this observation to the laboratory: numerical simulations typically produce a more noisy environment than is actually the case in the laboratory (thus, allowing the gyrotron mode to start with higher power), and so tends to exaggerate the potential for mode competition. However, if priming is the reason for the absence of the gyrotron mode, it could be easily included in the laboratory. We shall investigate this issue in the future.

In summary, we have carried out time-dependent, PIC computer simulations of a CARM in a realistic 3-D oscillator configuration. Simulations of the NRL 100 GHz CARM oscillator experiment suggest that the efficiency at the

experimental parameters is intrinsically low; even when no mode competiton is present, the efficiency is only about 3%. The most effective way to achieve higher efficiency appears to be to reduce or taper the magnetic field. In particular, it is shown the oscillator could produce 24 MW power with a 3% beam velocity spread by using a beam current of 400 A and tapering the magnetic field down by 20% along the length of the cavity. The absence of gyrotron mode competition when the oscillator is primed with the desired CARM mode raises the possiblity that priming could be beneficial in the laboratory in discriminating against unwanted longitudinal as well as transverse modes.

Acknowledgments

This work was supported by the USAF, under grant AFOSR 88-0027, the National Science Foundation under contract ECS86-03644, and the San Diego Supercomputing Center.

References

1. V.L. Bratman, G.G. Denisov, N.S. Ginzburg, and M.I. Petelin, IEEE J. Quantum Electron. QE-19, 282 (1983).

2. J.L. Vomvoridis, Int. J. Electron. 53, 555 (1982).

3. A.T. Lin, Int. J. Electron. 57, 1097 (1984).

4. Arne W. Fliflet, Int. J. Electron. 61, 1049 (1986).

5. T.H. Kho and A.T. Lin, Phys. Rev. Lett. 59, 1181 (1987); Nucl. Instrum. Methods A272, 574 (1988).

6. I.E. Botvinnik, V.L. Bratman, A. B. Volkov, G.G. Denisov, B.D. Kol'chugin, and M.M. Ofitserov, Sov. Tech. Phys. Lett. 8, 596 (1982).

7. I.E. Botvinnik, V.L. Bratman, A.V. Volkov, N.S. Ginburz, G.G. Denisov, B.D. Kol'chugin, M.M. Ofitserov, and M.I. Petelin, JETP Lett. 35, 516 (1982).

8. R.B. McCowan, A.W. Fliflet, S.H. Gold, V.L. Granatstein, and M.C. Wang, Int. J. Electron 65, 463 (1988).

9. S.H. Gold, private communications.

10. M. Caplan, Ph.D dissertation, Dept. of Physics, Univ. Calif. Los Angeles, PPG-963 (1986).

11. A.T. Lin, Z.H. Yang, and K.R. Chu, IEEE Trans. Plasma Sci. 16, 129 (1988).

12. J.M. Dawson and A.T. Lin, "Basic Plasma Physics," edited by M.N. Rosenbluth and R.Z. Sagdeev (New York, North-Holland, 1984), Vol. II, chap. 7, p.555.

13. T.H. Kho and A.T. Lin, Phys. Rev A 40, 2486 (1989).

Table 1: Experimental Parameters

Beam voltage [kV]	600
Beam current [A]	200
Axial velocity spread	$\Delta v_z/v_z < 3\%$
Magnetic field B_o [kG]	25
Operating mode	TE_{61}
$\alpha = v_\perp/v_z$	0.6
Cavity parameters:	
Mean wall diameter [cm]	1.59
Upstream reflector	
Length [cm]	3.0
Ripple depth [mm]	0.25
Ripple period [mm]	1.68
Reflectivity	99%
Downstream reflector	
Length [cm]	1.5
Ripple depth [mm]	0.31
Ripple period [mm]	1.68
Reflectivity	90%
Center Section Length [cm]	2.6

Table 2: Efficiency dependence on current

Current [A]	200	300	600	1000	2000
Efficiency [%]	3.3	5.5	6.0	6.0	5.0
Growth rate [MHz]	40	184	313	558	757

Table 3: Efficiency dependence on interaction length

Length [cm]	7.1	9.7	12.3
Efficiency [%]	3.3	6.0	5.0
Growth rate [MHz]	40	290	422

Table 4: Effieciency dependence on magnetic field detuning

Change in B-field [kG]	0.0	-2.0	-3.0	-4.0
Efficiency [%]	5.5	15.5	21.5	0.0

Table 5: Efficiency dependence on magnetic field tapering

$\Delta B/B_o$	0.0	-0.1	-0.2	-0.25
Efficiency [%]	5.5	18.0	23.0	14.0

Table 6: Efficiency dependence on velocity spread

velocity spread [%]	0	1	3
Efficiency [%]	23.0	23.0	11.0

Figure Captions

Figure 1. Dispersion relation for the parameters in Table 1, showing the TE_{61} and cyclotron beam lines.

Figure 2. (a) Cross sectional view of electron beam; r_w is the cavity radius.

(b) Electron energies along the axis of cavity at steady state operation.

Figure 3. (a) Example of electric field profile along the cavity (arbitrary units).

(b) Temporal evolution of rf field energy, U(t) (arbitrary units), in cavity.

(c) Temporal dependence of spent electron beam energy.

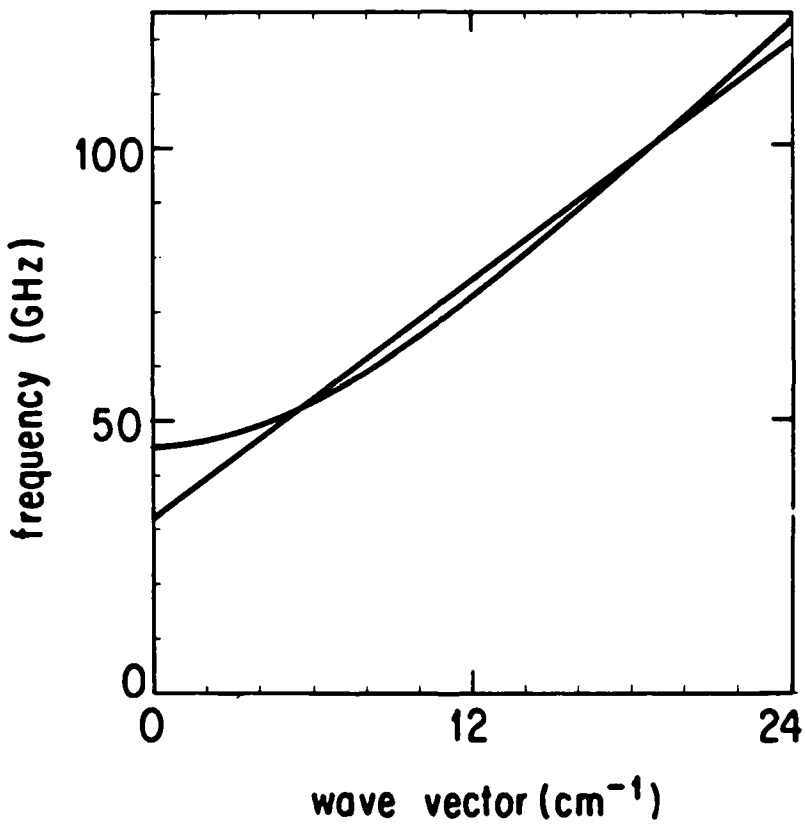

FIGURE 1

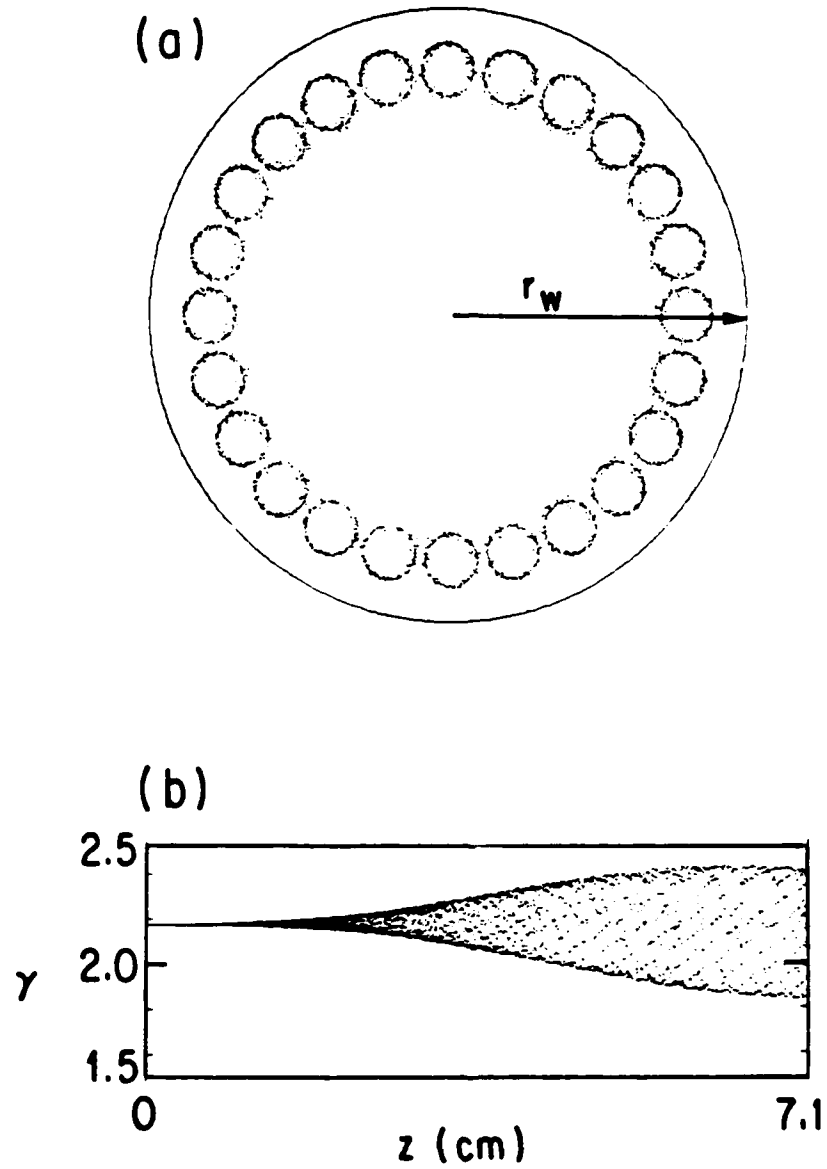

FIGURE 2

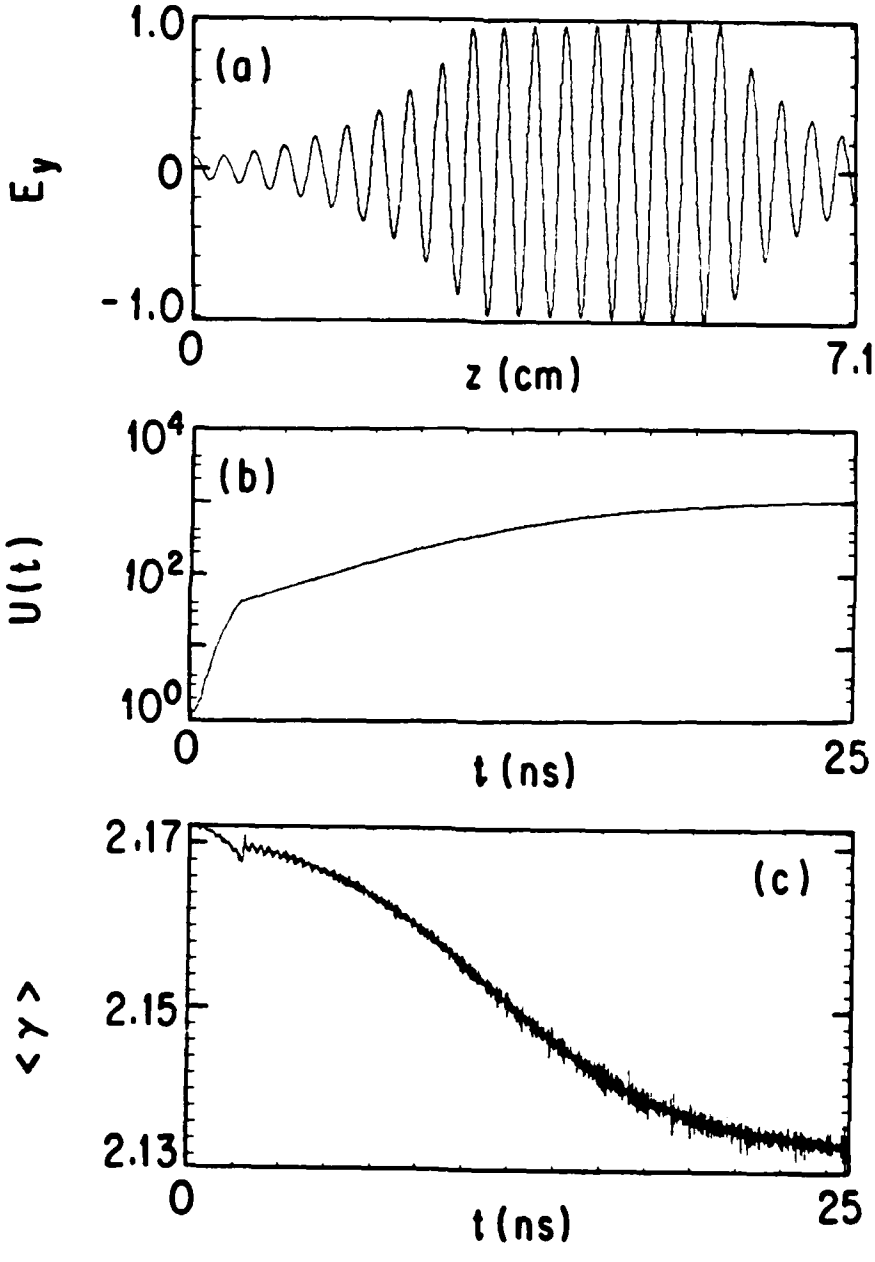

FIGURE 3

APPENDIX 3

Unified Theory and Comparative Study of CARMs, ICLs and FELs

K. R. Chen, J. M. Dawson, A. T. Lin and T. Katsouleas

University of California at Los Angeles
Department of Physics
Los Angeles, CA 90024 USA

Abstract

A unified small-signal amplification theory is developed to compare growth mechanisms responsible for a number of relativistic radiation generators. The theory is formulated from the basis that the electron resonance frequency produced by the external fields of the devices depends on γ^{-q}, where γ is the beam Lozentz factor and q is a constant ($q = 1$ for cyclotron autoresonance masers, $q = 1/2$ for ion-channel lasers and $q = 0$ for free electron lasers). It is concluded that for wave amplification, the sign of the electron mismatch frequency is required to be the same as the sign of bunching parameter which is determined by the total bunching both axial and azimuthal; this depends on the q value. The two bunching mechanisms exist, not only in the single electron resonance regime, but also in the collective gain regime. Competition or reinforcement between the two bunching mechanisms is determined by the q value, the electron axial velocity and the wave phase velocity.

PACS numbers: 42.52.+x, 42.55.Tb, 52.40.Mj, 52.75.Ms

I. Introduction

Electron bunching is the amplification mechanism responsible for many state of the art devices for generating radiation from microwaves to the ultraviolet. Among the many available devices, cyclotron masers (CARMs and gyrotrons) and free electron lasers (FELs) are the most successful.

Electron cyclotron maser instabilities, independently proposed by Twiss[1], Schneider[2] and Gaponov[3] in the late 50's, involve electrons gyrating about an external axial magnetic field. At the same time Weibel[4] studied electron whistler instabilities driven by an anisotropic velocity distribution of electrons. Both involve the transverse electromagnetic wave fields interacting with gyrating electrons. Two decades later, Chu and Hirshfield[5] presented a unified dispersion relation and pointed out that net bunching resulted from a competition between azimuthal (bunching due to cyclotron frequencies changes associated with the relativistic mass effect) bunching and axial (conventional overtaking) bunching is responsible for these instabilities. Bratman et al.[6] and Lin[8] investigated the electron cyclotron maser with emphasis on the Doppler shift effect (the so called cyclotron autoresonance maser or CARM).

In the late 50's and early 60's, Motz and Nakamura[13] and Phillips[14] studied the radiation mechanism for an electron beam going through a periodic undulators. In 1971 Madey[15] described the stimulated emission mechanism of a free electron laser based on a relativistic electron beam moving through a periodic transverse dc magnetic field and later carried out successful experiments in 1976[16] and 1977[17] at Stanford. Colson[18] presented a one-body analysis of the FEL by solving the pendulum equation. Dispersion relations have been derived for the collective regime of the FEL by Sprangle et al.[19]. Computer simulations by Kwan et al.[20], Lin and Dawson[21] and Liewer et al.[22] have been used to check linear theory, nonlinear saturation mechanisms and effeciencies of FELs.

CARMs[1]-[12] and FELs[13]-[24] have independently been the subjects of continuous activity for the past three decades. However, the similarities and differences between the two amplification mechanisms involved remain to be further clarified.

Recently the Ion-Channel Laser (ICL) as another means to generate tunable coherent radiation was conceived[25,26]; in this device a relativistic electron beam is injected into an underdense plasma (the plasma density is less than or equal to the beam density). The beam front pushes out the plasma electrons leaving an ion channel. Ion focusing causes the beam electrons to oscillate about the axis and plays a similar role as the magnetic field in a CARM. Using this type of device it appears that radiation can be produced with wave frequencies ranging from microwaves to soft X-rays; different devices must be used for different frequency ranges.

This study is motivated by growing activity on relativistic devices and was also triggered by findings on the amplification mechanism of ICLs. The goal is to develop a unified small-signal gain theory to illuminate the physical issues associated with the amplification mechanisms of CARMs, FELs and ICLs, and to place them on a common ground. The electron beams being studied are mono-energetic, have no velocity spread and gyrate along their drifting direction. The electromagnetic wave is assumed to be right circularly polarized and its amplitude is small enough to validate perturbation theory. The rate of electron energy change and the wave energy gain are evaluated to illustrate the amplification mechanism.

CARMs, ICLs and FELs all have a zeroth order radial force on the electrons which induces oscillatory motion about their overall drift. The resulting electron frequencies have different dependencies on the electron relativistic factor, depending on γ^{-q}. The value of exponents $(-q)$ of γ reveals different degrees of azimuthal bunchings caused by the electron relativistic mass variation. Also FELs differ from CARMs and ICLs in that they have an additional axial pondermotive force induced by the magnetic wiggler.

Some interesting physics insights will be discussed. Both inertial bunching and

force bunching[6,7] are included in our calculation. Force bunching can be neglected under some conditions. The inertial bunching has two parts : azimuthal bunching and axial bunching. The axial force will not give rise to electron axial density bunching if initially the electrons have uniform azimuthal phases. As a result there will be no space charge force. The azimuthal bunching which relies on relativistic effect is induced by the wave electric field. On the other hand, the axial bunching is a result of the competition between the conventional $v \times B$ force and the axial velocity change caused by the relativistic mass variation. For CARMs and ICLs, the relativistic mass variation effect on the axial velocity is dominant if

$$c^2 < v_{0z} v_{ph} \tag{1}$$

where c is the speed of light, v_{0z} is the beam axial velocity and v_{ph} is the phase velocity of wave. This is because the beam velocity is greater than the wave group velocity. We will show that for FELs the conventional $v \times B$ force is always dominant due to the pondermotive force of a magnetic wiggler.

The competition of different bunching mechanisms can be seen not only in the single electron resonance condition[5], but also in the rate of electron energy change. Azimuthal bunching and axial bunching do not always offset each other as concluded in[5]. If condition (1) is satisfied, they may reinforce each other. The competition will be shown to depend on the beam axial velocity v_{0z} (and/or energy) for ICLs, but is independent of v_{0z} for CARMs.

By evaluating the electron phase change[9,27] and using perturbation theory, we have developed a unified small-signal theory which gives a same formulation for CARMs, ICLs and FELs and reveals the general characteristics for relativistic radiation generation. The first order results contain the physical meaning of azimuthal and axial bunchings while the rate of electron energy change and the wave energy gain can be obtained from second order results ($< \vec{v_1} \cdot \vec{E}_1 >$) which also show the competition of the different bunching mechanisms. The same result can also be obtained by evaluating

the phase shift of an electron relative to its resonance phase with a wave. In Section III., the similarities and differences among CARMs, ICLs and FELs are illustrated through our unified theory. Section IV. gives a summary and discussion.

II. Unified Small-Signal Theory for Relativistic Radiation

Consider an electron undergoing transverse oscillation as it moves along the axial direction. There is a zeroth order force in the radial direction which may come from an axial magnetic field $\vec{B}_0$ as in CARMs, a transverse electric field $\vec{E}_i$ as in ICLs or a wiggler magnetic field $\vec{B}_w$ as in FELs. For simplicity, assume the force is centripetal which results in the electron motion having a helical trajectory. As shown in Fig.1. the radial force and electron velocity can be expressed by

$$\vec{F} = F[-\hat{x}\cos\phi - \hat{y}\sin\phi] \tag{2}$$

$$\vec{v} = v_\perp[-\hat{x}\sin\phi + \hat{y}\cos\phi] + v_z\hat{z} \tag{3}$$

where $\phi = \omega_s t + \phi_0$ is the electron oscillatory (azimuthal) phase angle, $\phi_0 = \phi(t = 0)$, $\omega_s = \omega_e/\gamma^q$ is the electron oscillating frequency which is dependent on its Lorentz factor $\gamma = (1 - v_\perp^2/c^2 - v_z^2/c^2)^{-\frac{1}{2}}$ with exponent $-q$, ω_e is the non-relativistic electron oscillating frequency, $F = \gamma m_e v_\perp \omega_s$ is the amplitude of the radial force, m_e is the electron rest mass, $v_\perp$ is the amplitude of the electron transverse velocity, and v_z is the electron axial velocity. Following common assumption we assume that the electron beam is tenuous, thus electron space charge is not important and the role of electrostatic waves[10] can be ignored in the amplification mechanism. We consider a right circularly polarized plane electromagnetic wave; its Doppler shifted frequency is comparable to the electron oscillation frequency:

$$\vec{E}_1 = E_1[\hat{x}\cos(\omega t - kz) + \hat{y}\sin(\omega t - kz)] \tag{4}$$

$$\vec{B}_1 = B_1[-\hat{x}\sin(\omega t - kz) + \hat{y}\cos(\omega t - kz)] \tag{5}$$

where $E_1(B_1)$ is the amplitude of wave electric (magnetic) field, ω is the wave frequency, $\vec{k} = k\hat{z}$ is the wavenumber and z is the axial spatial position, $v_{ph} = \omega/k$ is the wave phase velocity.

At this point, we have not introduced any ordering. Under these assumptions, the governing equations for an electron interacting with the wave are

$$\frac{d}{dt}(\gamma m_e c^2) = -eE_1 v_\perp \sin(\omega t - kz - \phi) \tag{6}$$

$$\frac{d}{dt}\vec{P}_\perp = -e\vec{E}_1(1 - \frac{kv_z}{\omega}) + \vec{F} \tag{7}$$

$$\frac{d}{dt}P_z = -\frac{e}{c}(\vec{v_\perp} \times \vec{B}_1) + F_p \tag{8}$$

$$\frac{d}{dt}z = v_z \tag{9}$$

where $-e$ is the electron charge, $\vec{P}_\perp = \gamma m_e \vec{v_\perp}$ is the electron transverse momentum, $F_p = 0$ for CARMs and ICLs, $F_p = -\frac{e}{c}(\vec{v_\perp} \times \vec{B}_w)$ is the pondermotive force of magnetic wiggler for FELs, and $P_z = \gamma m_e v_z$ is the electron axial momentum. Here we should be aware that the exchange of energy between the wave and electrons is associated with changes in electron velocities.

By using Faraday's law $\vec{B}_1 = \frac{c}{\omega}(\vec{k} \times \vec{E}_1)$, the pondermotive force due to the wave magnetic field can be expressed by

$$-\frac{e}{c}(\vec{v_\perp} \times \vec{B}_1) = \frac{k}{\omega}\frac{d}{dt}\gamma m_e c^2 \quad . \tag{10}$$

In an FEL, as $v_\perp/c \propto \gamma^{-1}$, and from the definition of γ we obtain

$$\frac{dv_z}{dt} = \frac{(c^2 - v_z^2)}{v_z} \cdot \frac{1}{\gamma}\frac{d\gamma}{dt} \quad . \tag{11}$$

Comparing Eq.(11) with Eqs. (8) and (10) the pondermotive force of a magnetic wiggler can be written by

$$F_p = \frac{k_w}{\omega}\frac{d}{dt}\gamma m_e c^2 \tag{12}$$

where k_w is the wavenumber of the magnetic wiggler.

Combining Eqs.(10-12) and Eq.(8), the axial momentum equation becomes

$$\frac{d}{dt}P_z = \frac{1}{v_p}\frac{d}{dt}\gamma m_e c^2 \tag{13}$$

where $v_p = \omega/k$ for CARMs and ICLs and $v_p = \omega/(k + k_w)$ for FELs.

Now we are going to do ordering. Since E_1 is a small parameter, $eE_1 v_\perp/(\gamma m_e c^2) << 1$, the governing equations can be solved by iteration. To zeroth order, Eqs. (6)-(9) and (13) can be reduced to

$$\gamma = \gamma_0 \tag{14}$$

$$\vec{v_\perp} = v_{0\perp}[-\hat{x}\sin\phi + \hat{y}\cos\phi] \tag{15}$$

$$v_z = v_{0z} \tag{16}$$

$$\phi = \omega_{s0}t + \phi_0 \tag{17}$$

$$z = v_{0z}t + z_0 \tag{18}$$

where $\gamma_0 = (1 - v_{0\perp}^2/c^2 - v_{0z}^2/c^2)^{-\frac{1}{2}}$ is the unperturbed electron γ, $v_{0\perp}(v_{0z})$ is the amplitude of the unperturbed electron transverse (axial) velocity, $\omega_{s0} = \omega_c/\gamma_0^q$ is the unperturbed electron oscillatory frequency and z_0 is the initial electron axial spatial position while ϕ_0 is the initial electron azimuthal phase angle.

To obtain the first order solution for γ, we substitute Eqs. (17) and (18) into Eq. (6) and obtain

$$m_e c^2 \frac{d}{dt}\gamma = -eE_1 v_{0\perp}\sin[(\omega - kv_{0z} - \omega_{s0})t - (kz_0 + \phi_0)] \quad . \tag{19}$$

Substituting Eqs. (17), (18) and (19) into Eq. (13) yields the first order solution for v_z:

$$\gamma_0 m_e \frac{d}{dt}v_z = -eE_1 v_{0\perp}[\frac{1}{v_p} - \frac{v_{0z}}{c^2}]\sin[(\omega - kv_{0z} - \omega_{s0})t - (kz_0 + \phi_0)] \quad . \tag{20}$$

Substituting Eq. (19) into Eq. (7) and separating the equations for the changes of the perturbed electron transverse velocity and azimuthal phase angle gives

$$\frac{d}{dt}v_{\perp 1} = -\frac{eE_1}{\gamma_0 m_e}(1 - \frac{kv_{0z}}{\omega} - \frac{v_{0\perp}^2}{c^2})\sin[(\omega - kv_{0z} - \omega_{s0})t - (kz_0 + \phi_0)] \tag{21}$$

$$\frac{d}{dt}\phi = \frac{\omega_c}{\gamma^q} + \frac{eE_1}{\gamma_0 m_e v_{0\perp}}(1 - \frac{kv_{0z}}{\omega})\cos[(\omega - kv_{0z} - \omega_{s0})t - (kz_0 + \phi_0)] \quad . \tag{22}$$

Eqs. (19) and (20) are readily integrated to give γ and v_z to first order in E_1:

$$\gamma = \gamma_0 + \frac{eE_1 v_{0\perp}}{mc^2} \frac{\cos[(\omega - kv_{0z} - \omega_{s0})t - (kz_0 + \phi_0)] - \cos(kz_0 + \phi_0)}{\omega - kv_{0z} - \omega_{s0}} \quad (23)$$

$$v_z = v_{0z} + \frac{eE_1 v_{0\perp}}{\gamma_0 mc^2}\left[\frac{c^2}{v_p} - v_{0z}\right] \frac{\cos[(\omega - kv_{0z} - \omega_{s0})t - (kz_0 + \phi_0)] - \cos(kz_0 + \phi_0)}{\omega - kv_{0z} - \omega_{s0}} \quad . \quad (24)$$

Substituting Eqs. (23) and (24) into Eqs. (22) and (9) respectively and integrating Eqs. (21)-(22) and (9) yields the expression for the perturbed amplitude of the electron transverse velocity, its azimuthal phase angle and the axial phase position:

$$v_{\perp 1} = \frac{eE_1}{\gamma_0 m_e}\left(1 - \frac{kv_{0z}}{\omega} - \frac{v_{0\perp}^2}{c^2}\right)\frac{\cos\psi - \cos(kz_0 + \phi_0)}{(\omega - kv_{0z} - \omega_{s0})} \quad (25)$$

$$\phi = \phi_0 + \omega_{s0}t - q\omega_{s0}\frac{eE_1 v_{0\perp}}{\gamma_0 m_e c^2} \left\{\frac{\sin\psi + \sin(kz_0 + \phi_0)}{(\omega - kv_{0z} - \omega_{s0})^2} - \frac{t\cos(kz_0 + \phi_0)}{\omega - kv_{0z} - \omega_{s0}}\right\} + \frac{eE_1}{\gamma_0 m_e v_{0\perp}}\left(1 - \frac{kv_{0z}}{\omega}\right)\frac{\sin\psi + \sin(kz_0 + \phi_0)}{\omega - kv_{0z} - \omega_{s0}} \quad (26)$$

$$z = z_0 + v_{0z}t + \left[\frac{c^2}{v_p} - v_{0z}\right]\frac{eE_1 v_{0\perp}}{\gamma_0 m_e c^2} \left\{\frac{\sin\psi + \sin(kz_0 + \phi_0)}{(\omega - kv_{0z} - \omega_{s0})^2} - \frac{t\cos(kz_0 + \phi_0)}{\omega - kv_{0z} - \omega_{s0}}\right\} \quad (27)$$

where $\psi = (\omega - kv_{0z} - \omega_{s0})t - (kz_0 + \phi_0)$. The perturbed amplitude of the electron transverse velocity $v_{\perp 1}$ and the fourth term of Eq. (26), ϕ_{1f} (the azimuthal phase variation due to forces acting on the electron in the radial direction), are called force bunching[6,7]. On the other hand, the axial phase variation z_1 and the third term of Eq. (26), ϕ_{1i} (the azimuthal phase variation due to the relativistic mass effect on the electron oscillatory frequency), are called inertial bunching because they are related to coordinate frame. ϕ_{1f} is generally greater than $v_{\perp 1}/v_{0\perp}$. From Eq. (26) the force bunching is negligible if $v_{0\perp}^2/c^2 >> (\omega - kv_{0z} - \omega_{s0})/\omega$, that is, when

$$\frac{\gamma_0^2 v_{0\perp}^2}{c^2} >> \frac{1}{\omega_{s0}t} \quad (28)$$

where $\omega_{s0}t \approx 2\pi \times$ the number of electron oscillation periods. This inequality is usually satisfied in regimes of interest.

For $(\omega - kv_{0z} - \omega_{s0})t \ll 1$, which is true for resonant interaction at early time, if we neglect the force bunching term, Eq. (26) and Eq. (27) can be further simplified to

$$\phi \simeq \phi_0 + \omega_{s0}t - q\omega_{s0}\frac{eE_1 v_{0\perp}}{\gamma_0 m_e c^2}\frac{t^2}{2}\sin(kz_0 + \phi_0) \tag{29}$$

$$z \simeq z_0 + v_{0z}t + [\frac{c^2}{v_p} - v_{0z}]\frac{eE_1 v_{0\perp}}{\gamma_0 m_e c^2}\frac{t^2}{2}\sin(kz_0 + \phi_0) \quad . \tag{30}$$

Although the first order solution gives no net energy exchange between the wave and electrons as can be seen by averaging Eq. (23) over the initial phases z_0 and ϕ_0 of all the electrons, it illustrates that the electrons are bunched in azimuthal phase. Eq. (29) reveals that at any position (e.g., $z_0 = 0$) electrons, initially from the upper half plane ($0 < \phi_0 < \pi$), slip back in phase due to the mass increase imparted by the wave electric force while the electrons initially from the lower half plane ($\pi < \phi_0 < 2\pi$) advance in phase due to the mass decrease; thus the electrons are bunched in azimuthal phase. Azimuthal bunching can occur in electron beams initially with uniform or coherent azimuthal phase distribution. As implied by Eq. (30), only for nonuniform phase angle plasmas does the axial force produce axial spatial bunching. On the other hand, the axial force will not give rise to a spatial bunching for uniform phase angle plasmas. This is because after taking the initial azimuthal phase angle average the density perturbation becomes zero even though every individual electron has been spatially perturbed. However the change in electron axial position will result in azimuthal phase bunching with respect to the wave through the Doppler effect. Since energy exchange involves phase perturbation, both azimuthal (relativistic) bunching and axial (conventional) bunching can play an important role in determining the rate of electron energy change to second order.

To second order the energy change is

$$\frac{d}{dt}\gamma m_e c^2 = -eE_1 v_{0\perp}\sin\psi - eE_1[-v_{0\perp}kz_1\cos\psi - v_{0\perp}\phi_1\cos\psi + v_{\perp 1}\sin\psi] \tag{31}$$

where $\phi_1 = \phi_{1i} + \phi_{1f}$.

Substituting Eqs. (25)-(27) into Eq. (31), we obtain the rate of electron energy change to second order in E_1:

$$\begin{aligned}\frac{d}{dt}\gamma m_e c^2 = -eE_1 v_{0\perp} \quad \{ \quad & \sin\psi \\ & + \frac{eE_1 v_{0\perp}}{\gamma_0 m_e c^2}[q\omega_{s0} - k(\frac{c^2}{v_p} - v_{0z})] \\ & \quad [\frac{\sin\psi\cos\psi + \sin(kz_0+\phi_0)\cos\psi}{(\omega - kv_{0z} - \omega_{s0})^2} \\ & \quad -\frac{t\cos(kz_0+\phi_0)\cos\psi}{(\omega - kv_{0z} - \omega_{s0})}] \\ & - \frac{eE_1}{\gamma_0 m_e}(1 - \frac{kv_z}{\omega}) \\ & \quad \frac{\sin\psi\cos\psi + \sin(kz_0+\phi_0)\cos\psi}{(\omega - kv_{0z} - \omega_{s0})} \\ & + \frac{eE_1}{\gamma_0 m_e}(1 - \frac{kv_z}{\omega} - \frac{v_{0\perp}^2}{c^2}) \\ & \quad \frac{\sin\psi\cos\psi - \cos(kz_0+\phi_0)\sin\psi}{(\omega - kv_{0z} - \omega_{s0})} \quad \} \quad . \end{aligned} \tag{32}$$

Eq. (32) is the expression for the energy exchange rate for a single electron whose initial azimuthal (axial) phase angle (position) is at ϕ_0 (z_0). To obtain the rate of net electron energy change, we integrate Eq. (32) over ϕ_0 and kz_0 :

$$\begin{aligned}\langle\frac{d}{dt}\gamma m_e c^2\rangle &= \frac{1}{4\pi^2}\int_0^{2\pi} d\phi_0 \int_0^{2\pi} dkz_0 (\frac{d}{dt}\gamma m_e c^2) \\ &\simeq -\frac{e^2 E_1^2 v_{0\perp}^2}{2\gamma_0 m_e c^2}[q\omega_{s0} - k(\frac{c^2}{v_p} - v_{0z})] \\ &\qquad [\frac{\sin(\omega - kv_{0z} - \omega_{s0})t}{(\omega - kv_{0z} - \omega_{s0})^2} - \frac{t\cos(\omega - kv_{0z} - \omega_{s0})t}{\omega - kv_{0z} - \omega_{s0}}] \\ &\qquad + \frac{e^2 E_1^2}{2\gamma_0 m_e}[2(1 - \frac{kv_z}{\omega}) - \frac{v_{0\perp}^2}{c^2}]\frac{\sin(\omega - kv_{0z} - \omega_{s0})t}{(\omega - kv_{0z} - \omega_{s0})} \quad . \end{aligned} \tag{33}$$

Wave is saturated when $< \frac{d}{dt}\gamma m_e c^2 >= 0$. Thus, the saturation time $T_{sat} \sim 4.4/(\omega - kv_{0z} - \omega_{s0})$ can be estimated by setting the inertial bunching term (the first term of the right hand side of Eq. (33)) to zero if we neglect the force bunching term. The second

term is caused by force bunching and vanishes for $\gamma_0 v_{0\perp}/c \sim 1$. $(\omega - kv_{0z} - \omega_{s0})t$ is approximately π at saturation, so taking $(\omega - kv_{0z} - \omega_{s0})t$ of order 1 we find that the force bunching term can be neglected once $\gamma_0^2 v_{0\perp}^2/c^2 >> 1/(\omega_{s0}t)$. This is the same condition found previously (Eq. 28). From now on, we will drop the force bunching term. The time-dependent change of the mean electron energy can be expressed as

$$(\overline{\gamma} - \gamma_0)m_e c^2 \simeq \frac{e^2 E_1^2 v_{0\perp}^2}{\gamma_0 m_e c^2}[q\omega_{s0} - k(\frac{c^2}{v_p} - v_{0z})] \frac{\cos(\omega - kv_{0z} - \omega_{s0})t - 1 + \frac{(\omega - kv_{0z} - \omega_{s0})t}{2}\sin(\omega - kv_{0z} - \omega_{s0})t}{(\omega - kv_{0z} - \omega_{s0})^3} \quad (34)$$

From energy conservation, multiplying $(\gamma_0 - \overline{\gamma})m_e c^2$ by the total number of electrons $n_e V$ and divided by the total wave energy $2E_1^2 V/8\pi$, where n_e is the electron density and V is the volume of interaction regime, yields the gain expression:

$$Gain \simeq -\frac{\omega_{pe}^2 v_{0\perp}^2}{\gamma_0 c^2}[q\omega_{s0} - k(\frac{c^2}{v_p} - v_{0z})]\frac{\cos\delta t - 1 + \frac{\delta t}{2}\sin\delta t}{\delta^3} \quad (35)$$

$$\simeq \frac{\omega_{pe}^2 v_{0\perp}^2 \omega}{24\gamma_0 c^2} t^4 \mathcal{B}\,\delta \qquad for \quad \delta t \ll 1 \quad (36)$$

$$\mathcal{B} \simeq q(1 - \frac{v_{0z}}{v_p}) - (\frac{c^2}{v_p^2} - \frac{v_{0z}}{v_p}) \quad (37)$$

$$\delta = \omega - kv_{0z} - \omega_{s0} \quad (38)$$

where $\mathcal{B}$ is the bunching parameter, δ is the frequency mismatch factor and $\omega_{pe} = (4\pi n_e e^2/m_e)^{\frac{1}{2}}$ is the electron plasma frequency. Eqs. (35)- (38) explicitly express the gain as a function of the electron beam energy γ_0, the electron azimuthal velocity $v_{0\perp}$, the electron plasma frequency ω_{pe}, the wave frequency ω, the mismatch δ and the bunching parameter $\mathcal{B}$. At the beginning of the interaction the gain is proportional to the 4th power of the time. As the interaction length is fixed, the gain is maximum at $\delta t \sim 2.6$ and proportional to the cubic power of the time.

The mismatch $\delta = \omega - kv_{0z} - \omega_{s0} \sim 0$ indicates how closely the electrons are to resonance with the wave. It also gives the wave frequency scaling:

$$\omega \sim 2\gamma_{0z}^2 \frac{\omega_e}{\gamma_0^q} \quad (39)$$

where $\gamma_{0z} = 1/(1 - v_{0z}^2/c^2)^{\frac{1}{2}}$ and we have assumed that the wave phase velocity and the beam velocity are near the speed of light. Eq. (39) shows that to attain high frequency radiation for $q < 2$ high electron oscillatory frequency or high energy electron beams have to be employed. But as indicated in Eq. (35) the increase in beam energy results in lower gain. Thus a practical choice for a high frequency radiation source is to use very high electron oscillatory frequency and moderate electron beam energy.

Eq. (36) also indicates that to achieve wave amplification the mismatch and the bunching parameter must have the same sign. Therefore, the bunching parameter B and mismatch factor δ should be carefully chosen in order to give positive gain. Their relation is shown in Table 1. There are two bunching mechanisms (azimuthal and axial bunchings) involved in the bunching parameter. The physical mechanism associated with the bunching parameter and mismatch factor can be also seen by examining the resonance condition

$$\omega - kv_z \mp \frac{\omega_e}{\gamma^q} = \delta \sim 0 \quad . \tag{40}$$

Instead of defining the Doppler shift frequency of wave as $\omega - kv_z$, for convenience we define the Doppler shifted frequency of an electron to be

$$\omega_D = kv_z \pm \frac{\omega_e}{\gamma^q} \tag{41}$$

which is the electron oscillatory frequency related to wave in the beam frame. By interacting with the wave the electron axial velocity and energy change which results in

$$\Delta\omega_D = k\Delta v_z \mp q\frac{\omega_e}{\gamma_0^{q+1}}\Delta\gamma \tag{42}$$

where $\Delta\omega_D = \omega_D(t = \Delta t) - \omega_D(t = 0)$, $\Delta v_z = v_z(t = \Delta t) - v_z(t = 0)$, $\Delta\gamma = \gamma(t = \Delta t) - \gamma_0$ and we have assumed that the perturbation is small (i.e., $\Delta\gamma \ll \gamma_0$). From Eq. (6), the energy change is

$$\Delta\gamma = -\frac{e}{m_e c^2}(\vec{v_{0\perp}} \cdot \vec{E}_1)\Delta t \quad . \tag{43}$$

From Eq. (6) and Eq. (13), we obtain the axial velocity change:

$$\Delta v_z = -(\frac{c^2}{v_p^2} - \frac{v_z}{v_p})[\frac{\epsilon v_p}{\gamma_0 m_e c^2} \vec{v_{0\perp}} \cdot \vec{E_1}]\Delta t \quad . \tag{44}$$

Substituting Eqs. (43) and (44) into Eq. (42) and using the resonance condition (40) yield

$$\Delta\omega_D = \mathcal{B}\frac{\omega\ e}{\gamma_0 m_e c^2}(\vec{v_{0\perp}} \cdot \vec{E_1})\Delta t \tag{45}$$

which relates $\Delta\omega_D$ to the bunching parameter. We have also shown (Eq.37) that the same formula for the bunching parameter can be obtained by using small-signal gain theory.

The first term in the bunching parameter expression from the small-signal theory result (Eq. 37) comes from the variation of the electron azimuthal phase angle (Eq. 26) induced by interacting with the azimuthal electric field. Hence, the first term of the bunching parameter is called azimuthal bunching. On the other hand, the second term is called axial bunching. It comes from the variation of the electron axial phase position (Eq. 27) resulting from the perturbation of the axial velocity. The first term of the axial phase variation is due to the perturbation of the axial velocity by the nonrelativistic $\vec{v} \times \vec{B}$ force, but the second term is due to the relativistic mass variation. The axial bunching is the result of competition between the mass variation effect and the conventional $\vec{v} \times \vec{B}$ effect.

Figure. 2. shows the relations between the two bunching mechanisms in the plot v_p/c is the horizontal axis and v_{0z}/c as its vertical axis. It can be divided into four regions. In region (I), the beam velocity is greater than the phase velocity of the wave and separated from the others by the line $v_{0z} = v_p$. In this region azimuthal bunching reinforces axial bunching and the bunching parameter is negative ($\mathcal{B} < 0$). In region (II) and region (III) the two bunchings offset each other. Axial bunching is dominant and the bunching parameter is negative in region (II) while azimuthal bunching dominates and the bunching parameter is positive in region (III). These two regions are separated

by the curve

$$(1-q)\frac{v_{0z}}{c} = \frac{c}{v_p} - q\frac{v_p}{c} \quad . \tag{46}$$

As $v_{0z}/c \to 0$, v_p/c approaches $q^{-\frac{1}{2}}$ at the point P. On this curve, the bunching parameter $\mathcal{B}$ is zero and there is no radiation (Eq. 36). Using operating parameters slightly away from this curve to obtain a small but finite gain, the electrons can remain resonant with the wave for a long time since the two bunchings effects offset each other. This is called autoresonance. Region (IV) is separated from region (III) by the curve $1 = v_{0z}/c \cdot v_p/c$. On this curve the axial bunching term is zero because the bunching from the $\vec{v} \times \vec{B}$ force is exactly cancelled by that of the relativistic mass variation In region (IV), the relativistic mass variation effect on the axial bunching is dominant while the conventional $\vec{v} \times \vec{B}$ force effect is dominant in other regions. Hence the axial bunching reinforces azimuthal bunching and the bunching parameter is positive ($\mathcal{B} > 0$).

Although Eqs. (35)-(38) and (45) are derived by including relativistic mass variation, the derivations are still valid in the weakly relativistic limit $\gamma \to 1$. Competition between the two bunchings persists not only in relativistic beams but also in weakly relativistic plasmas. The relativistic (azimuthal) bunching may dominate for weakly relativistic electrons and the conventional (axial) bunching may dominate at very relativistic electron energies as implied by Fig. 2.

To obtain the time-dependent mismatch factor we rewrite the resonant condition (40) as

$$\delta(\Delta t) = \omega - \omega_D(t=0) - \Delta\omega_D \sim 0 \qquad \text{for} \quad \textit{resonance} \tag{47}$$

For wave amplification more electrons give up energy ($\vec{v_{0\perp}} \cdot \vec{E_l} > 0$) to the wave than take energy from it so that for most electrons $\Delta\omega_D$ and $\mathcal{B}$ must have the same sign (Eq. 45). In the case of positive (negative) $\mathcal{B}$, the majority of electrons increase (decrease) their Doppler-shifted frequency, that is, $\Delta\omega_D > 0$ (< 0). Therefore, an initial positive (negative) mismatch factor δ is essential in order to retain most electrons in

resonance with the wave at early time. This explains why the sign of the mismatch factor is required to be the same as the sign of the bunching parameter for wave amplification as shown in Table I.

III. the Comparison of CARMs, ICLs and FELs

In the previous section, a unified theory was developed to describe the general wave amplification process. In this section, the unified theory will be applied to different devices. In a CARM configuration (Fig.3a.) an external magnetic field ,B_0, is imposed along the axial direction. The centipetal radial driving force which makes electron gyrate comes from $v_{0\perp} \times B_0$ force. In this case $\omega_s = \omega_{ce}$ where $\omega_{ce} = eB_0/\gamma m_e c = \Omega_{ce}/\gamma$ is the electron cyclotron frequency, $q = 1$, and $F_0 = eV_{0\perp}B_0/c$ is the amplitude of the driving force. The resonance condition is

$$\omega - kv_z - \frac{\Omega_{ce}}{\gamma} \sim 0 \quad . \tag{48}$$

The resonant wave frequency is $\omega \sim 2\gamma_{0z}^2\Omega_{ce}/\gamma \sim 2\gamma\Omega_{ce}$ where we have assumed $v_{0z} \gg v_{0\perp}$. The rate of electron energy variation becomes

$$\langle \frac{d}{dt}\gamma m_e c^2 \rangle \simeq -\frac{e^2 E_1^2 v_{0\perp}^2 \omega}{6\gamma_0 m_e c^2} t^3 \mathcal{B}_c \delta_c \qquad for \quad \delta_c t \ll 1 \tag{49}$$

$$\mathcal{B}_c = (1 - \frac{v_{0z}}{v_{ph}}) - (\frac{c^2}{v_{ph}^2} - \frac{v_{0z}}{v_{ph}}) \tag{50}$$

$$= 1 - \frac{c^2}{v_{ph}^2}$$

$$\delta_c = \omega - kv_{0z} - \frac{\Omega_{ce}}{\gamma_0} \tag{51}$$

where $\mathcal{B}_c$ is the CARM bunching parameter and δ_c is the CARMs' mismatch factor. Here the results are general and include the bunching parameter dependence. In Ref. [9], a similar result was obtained except that the bunching parameter was equal to one which resulted from assuming $v_{0z} = 0$ and that the wave magnetic field $B_1 = 0$. Their calculation missed the competition between the two bunching mechanisms. Also, their coefficient 16 in the rate of energy change should be 24. This discrepancy arises because they neglected the cubic bunching part (Eq. 26 - 27). In Ref. [5], the bunching parameter is derived by examining the resonance condition and the result was the same

as the second line of Eq. (50). Their study concluded that the two bunchings always offset each other and the bunching parameter is independent of the beam drift velocity. This can only apply to regions (II) and (III) of Fig.2. In regions (I) and (IV), the two bunchings reinforce each other and autoresonance is impossible. However, region (II) and region (III) are separated by the $v_{ph} = c$ line, which is independent of the beam velocity. Here azimuthal (axial) bunching is dominant in the fast (slow) wave region.

In a circular polarized ICL configuration (Fig.3b.), the ion electric field which provides a centripetal driving force is represented by

$$\vec{E}_i = A_s \cdot r[\cos\phi\hat{x} + \sin\phi\hat{y}] \tag{52}$$

where $A_s = 2\pi n_i e$, n_i is the ion's density, r is the electron gyroradius, $A_s \cdot r$ is the amplitude of the ion electric field and ϕ is the angular phase angle. In this case $F_0 = 2\pi n_i e^2 r$ is the amplitude of the driving force, $v_{0\perp} = \omega_s r$, $q = \frac{1}{2}$ and $\omega_e = \omega_{ei} = 2\pi n_i e^2/m_e$. The resonance condition is

$$\omega - kv_z - \frac{\omega_{ei}}{\gamma^{\frac{1}{2}}} \sim 0 \quad . \tag{53}$$

The resonant wave frequency is $\omega \sim 2\gamma^{\frac{3}{2}}\omega_{ei}$. The rate of electron energy change and the gain are

$$\langle \frac{d}{dt}\gamma m_e c^2 \rangle \simeq -\frac{e^2 E_1^2 v_{0\perp}^2 \omega}{2\gamma_0 m_e c^2} \mathcal{B}_i [\frac{\sin\delta_i t}{\delta_i^2} - \frac{t\cos\delta_i t}{\delta_i}] \tag{54}$$

$$Gain \simeq -\frac{\omega_{pe}^2 v_{0\perp}^2 \omega}{2\gamma_0 c^2} \mathcal{B}_i \frac{2\cos\delta_i t - 2 + \delta_i t \sin\delta_i t}{\delta_i^3} \tag{55}$$

$$\mathcal{B}_i = \frac{1}{2}(1 - \frac{v_{0z}}{v_{ph}}) - (\frac{c^2}{v_{ph}^2} - \frac{v_{0z}}{v_{ph}}) \tag{56}$$

$$\delta_i = \omega - kv_{0z} - \frac{\omega_{ei}}{\gamma_0^{\frac{1}{2}}} \tag{57}$$

where $\mathcal{B}_i$ is the ICL bunching parameter and δ_i is the ICL mismatch factor. The gain formula is the essencially the same for a linear polarized ICL; it has a different coefficient because only one component of the electrons' transverse motion and the

wave field (Eq.2-5) are applied. $\mathcal{B}_i$ depends on the beam drift velocity while $\mathcal{B}_c$ is independent of it. In CARMs, when electrons interact with the wave, some electrons gain energy and some lose energy such that the mismatch factor varies in time, but the bunching parameter always remains constant. Thus, the electron will remain at the same region during the entire interaction. In that case, change of the mismatch sign may cause the saturation of wave amplification. However, in ICLs, the curve dividing region(II) and region(III) depends on the electron axial velocity. During ICL interaction, both the mismatch and bunching parameter are changing. It becomes possible for electrons from region(III) to enter into region(II) or vice versa after they have lost energy.

From Eq. (41) with the upper sign we know that if the electron's v_z is decreasing while its energy is decreasing, the resonance interaction can be prolonged to achieve higher efficiency. On the other hand, if v_z is increasing while its energy is decreasing, there will be no autoresonance; this is the case in region(IV) for CARMs and ICLs. From Eq. (13), we note that

$$\gamma_0 \frac{d}{dt} v_z = (v_g - v_{0z}) \frac{d}{dt} \gamma \tag{58}$$

where $v_g = c^2/v_{ph}$ is the group velocity of the wave. The first term on the right hand side of Eq. (58) is from the wave magnetic field (the $\vec{v} \times \vec{B}$ force), which converts the electron axial momentum to azimuthal motion. The second term comes from the wave electric field (the mass variation) , which increases the electron axial velocity as it dissipates the electron azimuthal energy. While the electron is losing its energy, and if $v_g < v_{0z} (v_g > v_{0z})$, its drifting velocity will be speeded up (slowed down); in other words, the electron always increases it's velocity (in absolute terms) relative to the wave. Thus, if the wave group velocity (e.g., a fast wave) is slower than the electron drifting velocity, that is,

$$c^2 < v_{0z} v_{ph} \quad , \tag{59}$$

then the change in axial velocity v_z (axial bunching) will not be able to compensate the change in energy (azimuthal bunching) to maintain the resonance. The competition of

the $\vec{v} \times \vec{B}$ effect and the mass variation effect on the axial velocity also exists in the bunching parameter and the rate of energy exchange.

In a circularly polarized FEL configuration (Fig.3c.), the helical undulator field is represented by

$$\vec{B_w} = B_w(\hat{x} \sin k_w z - \hat{y} \cos k_w z) \tag{60}$$

where B_w is the amplitude of the external magnetic wiggler and k_w is the wavenumber of the wiggler field. The radial driving force comes from the $v_{0z}\vec{} \times \vec{B_w}$ term. In this case $F_0 = \gamma_0 m_e v_{0\perp} k_w v_{0z}$ is the amplitude of the driving force, $v_{0\perp} = (eB_w)/(\gamma_0 m_e k_w c)$ is the electron azimuthal velocity, $q = 0$, $\omega_e = k_w c$, $\phi_0 = k_w z_0$ and $k \gg k_w$ for energetic electron beams ($v_{0z} \rightarrow c$). The resonance condition can be expressed by

$$\omega - k v_z - k_w c \sim 0 \tag{61}$$

which means that the resonant wave frequency is approximately $2\gamma_{0z}^2 k_w c$. The rate of electron energy change and the gain are

$$\langle \frac{d}{dt} \gamma m_e c^2 \rangle \simeq -\frac{e^2 E_1^2 v_{0\perp}^2 \omega}{6\gamma_0 m_e c^2} t^3 \mathcal{B}_f \delta_f \tag{62}$$

$$Gain \simeq -\frac{\omega_{pe}^2 v_{0\perp}^2 \omega}{2\gamma_0 c^2} \mathcal{B}_f \frac{2\cos\delta_f t - 2 + \delta_f t \sin\delta_f t}{\delta_f^3} \tag{63}$$

$$\mathcal{B}_f = 0 - (\frac{c^2}{v_p^2} - \frac{v_{0z}}{v_p}) \tag{64}$$

$$\delta_f = \omega - k v_{0z} - k_w c \tag{65}$$

where $\mathcal{B}_f$ is the FEL bunching parameter and δ_f is the FEL mismatch factor. The gain result can be recovered from Ref. [18], which is based on solving a pendulum equation, by letting $\mathcal{B}_f \simeq -1/\gamma_{0z}^2$. For an FEL ($q = 0$), the gyrofrequency of the electron is independent of the beam energy so that the point P (i.e., $v_{0z} \rightarrow 0$) in Fig.2. is at infinity. Region (III) vanishes and there is no azimuthal bunching.

Due to the pondermotive force (Eq. 12), the interaction of the wave and the electron

in the axial direction is changed to

$$\frac{d}{dt}v_z = c(\frac{c}{v_p} - \frac{v_{0z}}{c})\frac{d}{dt}\gamma \tag{66}$$

where $v_p = \omega/(k+k_w)$. We can rewrite $c(\frac{c}{v_p} - \frac{v_{0z}}{c})$ as $(v_g + v_{gp} - v_{0z})$ where $v_{gp} = c^2 k_w/\omega$. The pondermotive force of the magnetic wiggler enhances the EM wave $\vec{v_0} \times \vec{B_1}$ force. For practical purposes, the mismatch is made very small so that the electron drifting motion is synchronous with the pondermotive potential ($v_p \sim v_{0z}$). In this situation, $(\frac{c}{v_p} - \frac{v_{0z}}{c}) \simeq \frac{c}{v_{0z}}(1 - \frac{v_{0z}^2}{c^2}) \propto \frac{1}{\gamma_{0z}^2}$ and is always positive. Therefore, the change of the electron axial velocity v_z has the same sign as its energy change. The conventional $\vec{v} \times \vec{B}$ force is always larger than the mass variation effect in the axial bunching process.

Table II. summarizes the comparison. All the driving forces are transverse. Their *resonance conditions are similar but with different* q indices on the gyrofrequencies. The P points which separate region (II) and region (IV) are $1, \sqrt{2}$ and ∞ for CARMs, ICLs and FELs, respectively. Their rates of electron energy change are the same except for different bunching parameter and mismatch factor. FELs have the most favorable scaling for the output frequency with the beam energy ($\propto \gamma^2$), but the electron undulation frequency is limited by the available wiggler period. Thus it requires high γ to achieve high frequency lasing at the expense of reducing the gain. CARMs have the best controls on beam guiding and wave mode selection, but the radiation output frequency is only linearly proportional to γ and the electron gyration frequency is limited by the available magnet technology. ICLs can have the highest electron oscillation frequency (e.g., $\omega_{ei} \sim 10^3 GHz$ for $n_i \sim 10^{16} cm^{-3}$) and the output frequency scales more favorably than for CARMs, i.e., $\sim \gamma^{\frac{3}{2}}$. In addition to these advantages, ICLs do not require any applied external field.

IV. Summary and Discussion

We have developed a unified small-signal theory to describe the amplification mechanism in relativistic electronics. The mechanisms persist to nonrelativistic electron energies. This study unifies the amplification mechanisms of different wave emission devices by assuming that the electron oscillation frequencies depend on their beam energies as γ^{-q} where $q = 1, \frac{1}{2}$ and 0, respectively for CARMs, ICLs and FELs. Their differences basically come from different q values.

The azimuthal bunching which depends on the q value, electron drift velocity and wave phase velocity is induced by the wave electric field (E_1) and is a relativistic mass effect. On the other hand the axial bunching caused by the $\vec{v} \times \vec{B}$ force which is a nonrelativistic effect and the relativistic mass variation is independent of the q value. The bunching can take place in velocity space related to wave. It is not necessary for electrons to be bunched in real axially space to have wave amplification. The competing effects which cause bunching exist in both the single electron resonance condition and the collective rate of electron energy change. The azimuthal bunching is dominant over the axial bunching if $q(1 - \frac{v_{0z}}{v_p}) > (\frac{c^2}{v_p^2} - \frac{v_{0z}}{v_p})$, and vice versa. If $v_{0z} > v_p$ or $c^2 < v_{0z}v_p$, in stead of offsetting the two bunchings reinforce each other which results in no autoresonance. In order to have wave amplification the sign of the mismatch is required to be the same as the sign of the bunching parameter. For CARMs and ICLs the relativistic mass variation effect on the electron axial velocity may overwhelm the $\vec{v} \times \vec{B}$ force so that the change in axial velocity is opposite to the electron energy change and the axial bunching term becomes negative. For FELs the bunching arising from the relativistic mass variation is smaller than that of the pondermotive force from the wiggler and wave magnetic fields so that the FEL bunching parameter is always negative. All these mechanism can upshift the undulation frequency by a factor of $2\gamma_{0z}^2$. The ICL electron gyrofrequency $\omega_s = (2\pi n_i e^2)/(m_e \gamma^{\frac{1}{2}})$ can be made to be the highest

among the three with the present day technology. FELs and CARMs already have successful experimental results. ICLs are expected to become a realistic mechanism to generate coherent tunable radiations from the microwave regime to the soft X-ray regime.

The unified small-signal theory not only links the old physics issues in CARMs and FELs, but also reveals the new physics issues in ICLs. Any new mechanisms ought to be covered by the unified theory.

Acknowledgment

The authors wish to acknowledge K. R. Chu, C. S. Kou and K. C. Leou for many stimulated discussion. We also thank A. M. Sessler and D. H. Whittum for helpful discussion on ICL. This work is supported by the National Science Foundation, the Department of Energy, the Lawrence Livermore National Laboratory and the Air Force Office of Scientific Research.

References

[1] R. Q. Twiss, *Australian J. Phys.* 11, 564(1958).

[2] J. Schneider, *Phys. Rev. Lett.* 2, 504(1959).

[3] A. V. Gaponov, *Izv. Vyssh. Uchebn. Zaved., Radiofizi.* 2, 450, 836(1959).

[4] E. S. Weibel, *Phys. Rev. Lett.* 2, 83(1959).

[5] K. R. Chu and J. L. Hirshfield, *Phys. Fluids*, 21, 461(1978).

[6] V. L. Bratman, N. S. Ginzburg, G. S. Nusinovich, M. I. Petelin, and P. S. Strelkov, *Int. J. Electronics* 51, 541(1981).

[7] A. V. Gaponov, M. I. Petelin, and V. K. Yulpatov, *Izv. VUZov. Radiofizika [Radiaphysics and Quantum electronics]* 10, 1414(1967).

[8] A. T. Lin, *Int. J. Electronics* 57, 1097(1984).

[9] K. R. Chu, *J. of the Chinese Inst. of Eng.* 4, 85(1981).

[10] K. R. Chen and K. R. Chu, *IEEE Trans. Microwave Theory Tech.* 34, 72(1986).

[11] T. H. Kho and A. T. Lin, *Phys. Rev. Lett.* 59, 1181(1987).

[12] L. Chen, T. H. Kho, K. R. Chen and A. T. Lin, *phys. Fluids* 31, 3116(1988).

[13] H. Motz and M. Nakamura, *Ann. of Phys.* 7, 84(1959).

[14] R. M. Phillips, *I.R.E. Trans. Electron Devices* 7, 231(1960).

[15] J. M. J. Madey, *J. Appl. Phys.* 42 1906(1971).

[16] L. R. Elias, W. M. Fairbank, J. M. J. Madey, H. A. Schwettman and T. I. Smith, *Phys. Rev. Lett.* 36, 717(1976).

[17] D. A. G. Deacon, L. R. Elias, J. M. J. Madey, G. J. Ramian, H. A. Schwettman and T. I. Smith, *Phys Rev. Lett.* 38, 892(1977).

[18] W. B. Colson, *Physics of Quantum Electronics* 5, 157(1978).

[19] P. Sprangle, C. M. Tang and W. Manheimei, *Phys. Rev. Lett.* 43, 1932(1979).

[20] T. Kwan, J. M. Dawson and A. T. Lin, *Phys. Fluids* 20, 581(1977).

[21] A. T. Lin and J. M. Dawson, *Phys. Rev. Lett.* 42, 1670(1979).

[22] P. C. Liewer, A. T. Lin and J. M. Dawson, *Phys. Rev. A* 23, 1251(1981).

[23] W. B. Colson, *SPIE vol. 738 Free-Electron Lasers(1987).*

[24] C. W. Roberson and P. Sprangle, *Phys. Fluids B* 1, 1(1989).

[25] D. H. Whittum, A. M. Sessler and J. M. Dawson, *Phys. Rev. Lett.* 64, 2511(1990).

[26] K. R. Chen, T. Katsouleas and J. M. Dawson, to appear in *IEEE Trans. Plasma Sci.* (Oct. 1990).

[27] J. M. Dawson, *Phys. Fluids* 4, 869(1961).

Table.I. For wave emission the relation between bunching parameter and mismatch factor.

bunching parameter B	required mismatch δ	dominant bunching
positive	positive	azimuthal†
0	no wave emission	cancel
negative	negative	axial

† For FEL there is only an axial bunching and no azimuthal bunching.

Table.II. A brief comparison of CARMs, ICLs and FELs.

	CARMs	ICLs	FELs
driving force	$-\frac{e}{c}(\vec{v_{0\perp}} \times \vec{B_0})\hat{e_\perp}$	$-e\vec{E_i}\hat{e_\perp}$	$-\frac{e}{c}(\vec{v_{0z}} \times \vec{B_w})\hat{e_\perp}$
mismatch $\delta =$	$\omega - kv_z - \frac{\Omega_{ce}}{\gamma}$	$\omega - kv_z - \frac{\omega_{ei}}{\gamma^{\frac{1}{2}}}$	$\omega - kv_z - k_w c$
wave frequency	$2\gamma_0\Omega_{ce}$	$2\gamma_0^{\frac{3}{2}}\omega_{ei}$	$2\gamma_0^2 k_w c$
bunching parameter $\mathcal{B}$	azimuthal $\mathcal{B}_{az}$ — axial $\mathcal{B}_{ax}$	azimuthal $\frac{1}{2}\mathcal{B}_{az}$ — axial $\mathcal{B}_{ax}$	axial $-\mathcal{B}_{ax}$
$P = \sqrt{\frac{1}{q}}$	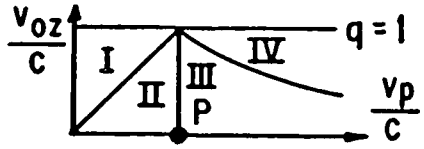	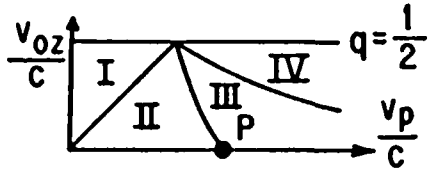	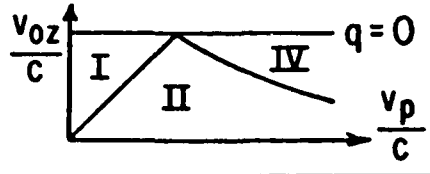
energy change	$-\alpha t^3 \mathcal{B}_c \delta_c$	$-\alpha t^3 \mathcal{B}_i \delta_i$	$-\alpha t^3 \mathcal{B}_f \delta_f$

where $\mathcal{B}_{az} = 1 - \frac{v_{0z}}{v_p}$, $\mathcal{B}_{ax} = \frac{c^2}{v_p^2} - \frac{v_{0z}}{v_p}$ and $\alpha = \frac{e^2 E_1^2 v_{0\perp}^2 \omega}{16\gamma_0 m c^2}$

Figure captions

Fig.1. A basic electron relativistic radiation model.

Fig.2. Relations between two bunching mechanisms in four v_{0z}/c vs. v_p/c regions.

Fig.3. The electron motion and external fields of CARM, ICL, and FEL. Their external forces play a similar role although the origin and direction of fields are quite different.

Fig.1.

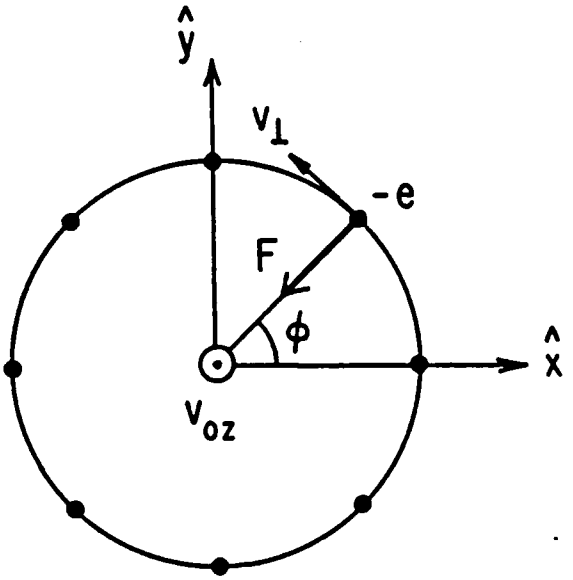

$$\phi = \omega_s t + \phi_0$$

Fig.2.

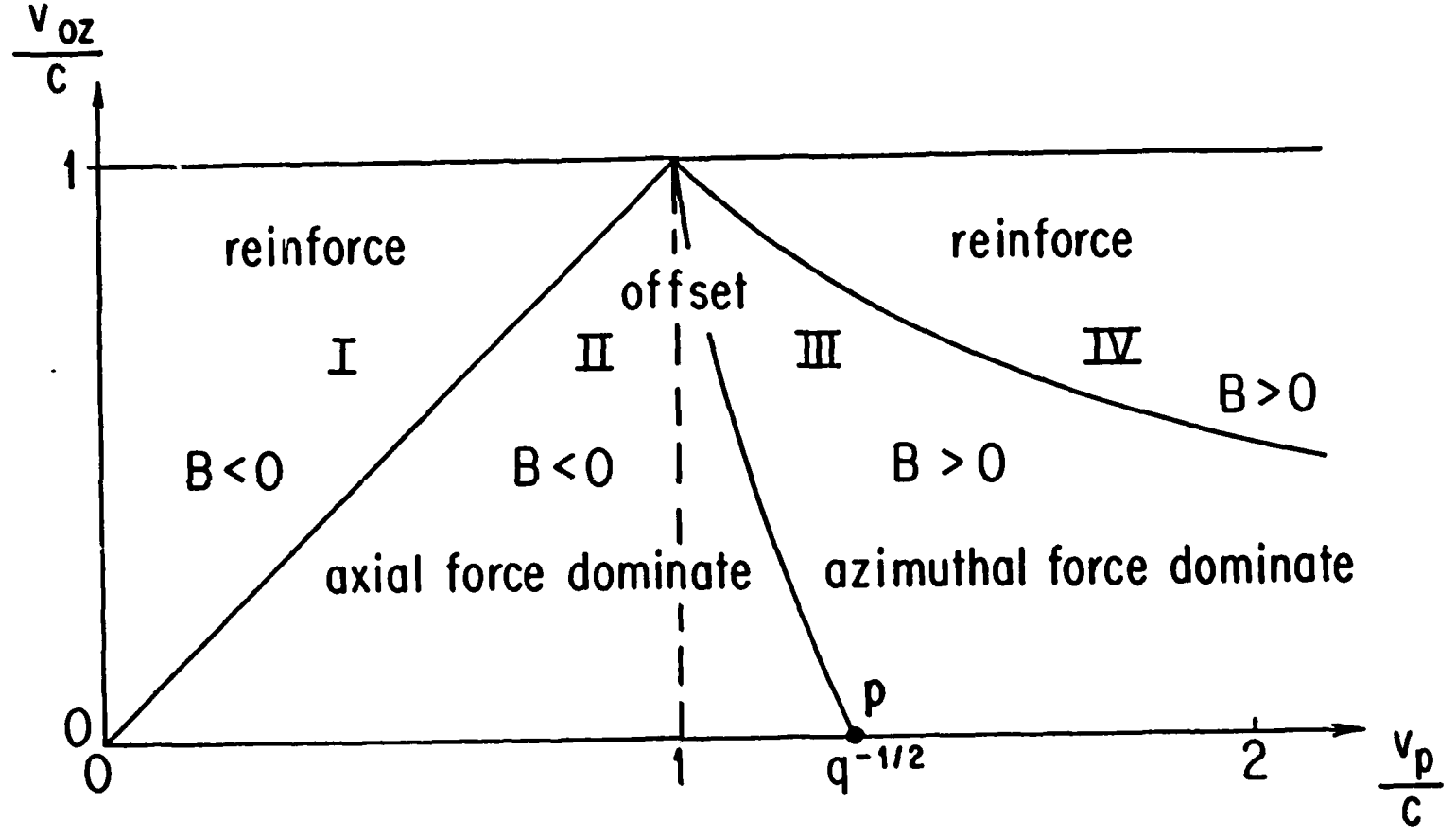
$\frac{V_{oz}}{c}$
1
reinforce
offset
reinforce
I
II
III
IV
B>0
B<0
B<0
B>0
axial force dominate
azimuthal force dominate
p
0
0
1
$q^{-1/2}$
2
$\frac{V_p}{c}$

Fig.3.

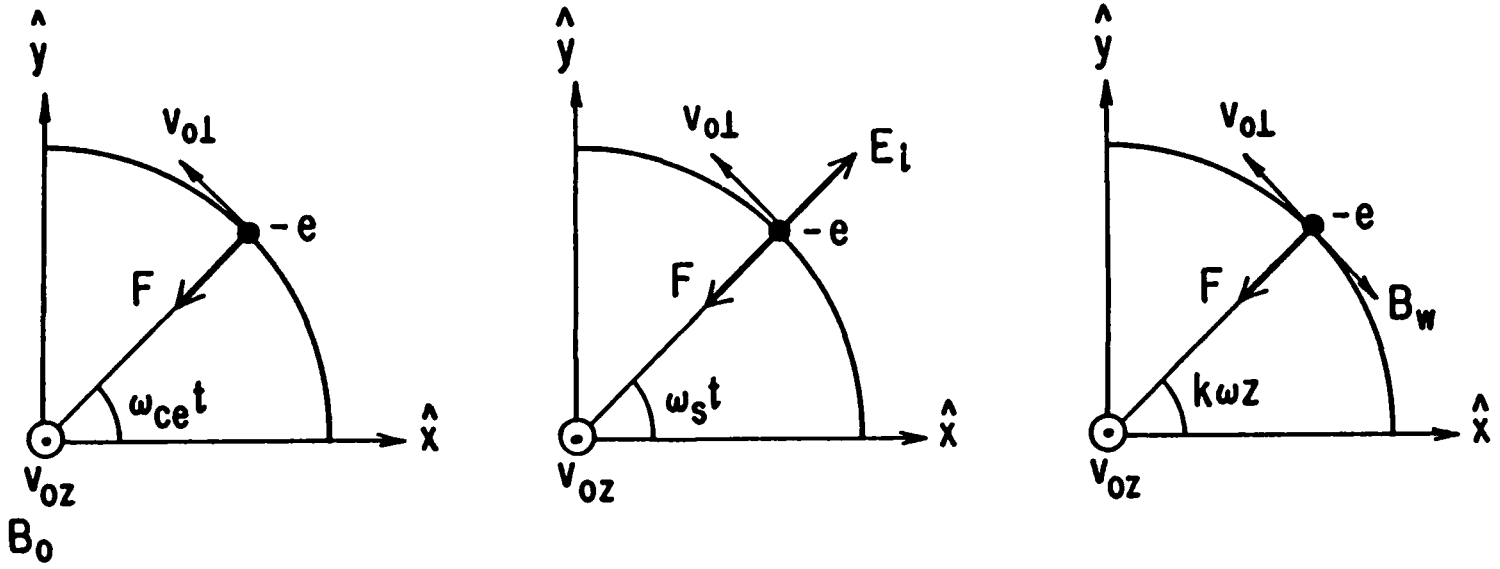
ŷ
$v_{o\perp}$
-e
F
$\omega_{ce}t$
x̂
v_{oz}
B_o
(a) CARM
ŷ
$v_{o\perp}$
E_i
-e
F
$\omega_s t$
x̂
v_{oz}
(b) ICL
ŷ
$v_{o\perp}$
-e
F
B_w
$k\omega z$
x̂
v_{oz}
(c) FEL